Photocopy and Use Authorization

In presenting this thesis in partial fulfillment of the requirements for an advanced degree at Idaho State University, I agree that the Library shall make it freely available for inspection. I further state that permission for extensive copying of my thesis for scholarly purposes may be granted by the Dean of the Graduate School, Dean of my academic division, or by the University Librarian. It is understood that any copying or publication of this thesis for financial gain shall not be allowed without my written permission.

Signature _____

Date _____

Quantifying and clustering lava flow morphologies at different data resolutions:

applications for terrestrial and planetary flows

By

Hester C. Mallonee

A thesis

submitted in partial fulfillment

of the requirements for the degree of

Master of Science in the Department of Geosciences

Idaho State University

Spring 2022

To the Graduate Faculty:

The members of the committee appointed to examine the thesis of Hester C. Mallonee find it satisfactory and recommend that it be accepted.

_____

Dr. Shannon Kobs Nawotniak,

Major Advisor

_____

Dr. Donna Delparte,

Committee Member

_____

Dr. Kevin Parker,

Graduate Faculty Representative

DEDICATION

I would like to thank my family for their unwavering love. Thank you so much for the support, encouragement, and patience. This would not have been possible without you, and I am so grateful.

Many thanks to my friends and coworkers for laughing with me and listening to me throughout this process. Thank you for keeping me in good spirits and letting me sleep on your couches throughout this adventure.

Finally, innumerable thanks to my advisor, Dr. Shannon Kobs Nawotniak. This thesis has been a long process, and would have failed without your patience, empathy, investment in both my academics and career, and brilliant insights. Thank you for not letting me give up.

ACKNOWLEDGEMENTS

This work was funded by the NASA FINESSE (Field Investigations to Enable Solar System Science and Exploration) project, led by Principal Investigator Dr. Jennifer L. Heldmann, which was funded by the NASA Solar System Exploration Research Virtual Institute (SSERVI). Additional support was received from the NASA BASALT (Biologic Analog Science Associated with Lava Terrains) project, led by Principal Investigator Dr. Darlene S. S. Lim, which was funded by the NASA Planetary Science and Technology through Analog Research (PSTAR) Program (NNH14ZDA001N-PSTAR) grant (14-PSTAR14_2-0007.) Fieldwork, including UAS data collection, was conducted at Craters of the Moon National Monument under Permit No. CRMO-2014-SCI-0004. UAS data was collected by Michael Downs of Kennedy Space Center and Dr. Donna Delparte of Idaho State University, with assistance from the author.

TABLE OF CONTENTS

LIST OF FIGURES

Quantifying and clustering lava flow morphologies at different data resolutions: applications for terrestrial and planetary flows

THESIS ABSTRACT – IDAHO STATE UNIVERSITY (2022)

Basaltic lava flow morphologies provide insight into the eruptive history of the volcano and the progression of a lava flow. However, classifying these morphologies is a subjective process. The goal of this work is to develop a quantitative method of describing lava flow roughness. Using Unmanned Aerial Systems, we created orthophoto mosaics and Digital Terrain Models. We then performed qualitative a priori classifications using aerial images, and selected areas that appeared to have a single morphology. We used the root-mean-square height and Area Ratio to calculate the quantitative roughness of these areas in three-dimensions; we then clustered the resulting roughness measurements using a clustering technique called the kmeans. We performed this analysis on data resolutions of 0.1, 0.5, 1, and 2 m/pixel to better simulate satellite data, as well as performing this analysis using both a scaling moving window and a static moving window. Endmember lava flow morphologies smooth pāhoehoe and blocky-'a'ā were easily identified by the method. Other clusters included small-scale roughness (slabby pāhoehoe), small-medium scale roughness (lobate, rubbly pāhoehoe), and medium-large scale roughness (rubbly-inflated, hummocky). Our quantitative method of differentiating lava flows could be applied to other lava flows, including those on Earth and other planetary bodies.

Keywords: lava flow, volcanology, planetary geology, basalt, roughness, terrain analysis

CHAPTER 1: INTRODUCTION

PROBLEM STATEMENT:

Identifying lava flow textures is crucial to understanding the emplacement conditions and eruptive history of the flow (Cashman et al., 1999; Guilbaud et al., 2007; Hon et al., 1994; Rowland et al., 1990; Self et al., 1998). Both in the field and for remote sensing analyses, identification of flow textures is typically conducted based on qualitative observations (Gregg et al., 2017; Harris et al., 2017; Hon et al., 1994; Keszthelyi et al., 2004; Lipman and Banks, 1987; Macdonald et al., 1953; Peterson and Tilling, 1980; Rowland and Walker, 1987); however, this identification method for classifying lava textures is inherently subjective, which can sometimes result in misidentified flow textures. The goal of this work was to employ statistical quantifications for the varying roughness in lava flow morphologies and to determine if individual morphologies can be found using objective clustering techniques.

The working hypothesis of this study was that various lava morphologies can be differentiated using measurements of surface roughness. Further, I anticipated that intermediate morphologies would be less distinguishable from one another and that distinguishing individual morphologies will be less feasible at coarser data resolutions. I tested these hypotheses using high-resolution Digital Terrain Models (DTMs) of lava flows from Craters of the Moon (COTM) National Monument and Preserve, Idaho, USA. Statistical measures of quantifying roughness included the root-mean-square (RMS) height and Area Ratio, and the clustering analysis was completed using the kmeans method. These methods show that some lava flow morphologies can be distinguished using quantitative methods, and at what data resolutions that distinction is feasible.

SCOPE OF WORK:

This work focuses on lava flow morphologies found in mafic and intermediate lava types found within the COTM lava field. We examine 33 sample areas each representing an individual lava flow morphology. Roughness is computed for each sample area using the RMS height and Area Ratio. Each sample area was downsampled to 0.1 m/pixel, 0.5 m/pixel, 1 m/pixel, and 2 m/pixel to investigate the effect of data resolution on morphological analyses. The RMS height and Area Ratio are found across these sample areas using a 3 pixel x 3 pixel moving window and an approximately 7 m x 7 m moving window to determine whether changing the moving window size affected the results. The sample areas are then grouped based on their roughness values using the kmeans clustering method. Using the kmeans clustering method allows textures to be quantitatively distinguished without bias.

ORGANIZATION OF THE THESIS:

This thesis is organized into five chapters. The first two (Introduction; Background) and last two chapters (Discussion and Future Work; Conclusions) are meant to serve as bookends for the central chapter, a manuscript intended for submission to a journal for publication. The bookending chapters are written for a more general audience and, particularly at the end, include more speculative ideas. Since the third chapter is meant to be able to stand alone as a document, content is repeated there in a more concise form.

CHAPTER 2: BACKGROUND:

THE CRATERS OF THE MOON LAVA FIELD:

The Craters of the Moon (COTM) lava field has a wide variety of lava flow morphologies and is an ideal location to study the roughness of such flows. It lies in southeast Idaho within the eastern Snake River Plain (ESRP) physiographic province. The ESRP is a large topographic depression, approximately 100 km wide by 400 km long (Hughes et al., 2002) and is the result of bimodal volcanism (Hughes et al., 1999). The subsurface contains significant quantities of rhyolite ignimbrites and rhyolite lavas associated with the Yellowstone hotspot eruptions (Pierce and Morgan, 1992). Following the emplacement of the rhyolitic deposits, there were subsequent basaltic flows, each ranging in size from 5 m to 25 m thick, that erupted from monogenetic shield volcanoes, as well as eruption of degassed rhyolite lava domes (Hughes et al., 1999). Stratigraphic relationships seen in deep borehole surveys near the towns of Kimama and Kimberly have allowed researchers to estimate a total thickness of 2,093 m for the ESRP basalt flows (Potter et al., 2019) with a volumetric output of 3.3 km^3/1000 years (Kuntz, 1992). The basaltic flows of the ESRP have characteristics of flood volcanism (sheet flows, eruptive fissures), as well as those more typical of shield volcanoes (lava tubes, lava channels, point sources); as such, Greeley (1982) proposed a new category of volcanism based on the ESRP called “plains-style volcanism.” The same style of volcanism has been found in both the Tharsis region (Greeley, 1982; Hauber et al., 2009) and the Elysium region (Plescia, 1993; Vaucher et al., 2009) on Mars.

Beginning 15,100 (+/- 160) years ago, basaltic lava flows in southeast Idaho began erupting from a series of fissures called the Great Rift (Kuntz et al., 2007). The Great Rift is the surface expression of a series of extensional zones that contain both eruptive and non-eruptive

fissures that run from southeast to northwest (Kuntz, 1992). These extensional zones accommodate regional Basin and Range strain and may be 15–20 km wide (Hughes et al., 2002). The magma source is at a depth of about 60 km in the mantle, with a reservoir near the Moho connected to an upper reservoir beneath the lava field by a series of fissures; a series of dikes leads to eruptive vents on the surface (Kuntz, 1992). The Great Rift is 85 km long and trends NW-SE (Kuntz, 1982) and includes the Kings Bowl lava field, the Wapi lava field, and the COTM field. The COTM is the largest of the Great Rift's lava fields, with an area of 1,600 km^2, and has experienced eight eruptive periods between 15,000 and 2,100 years ago (Kuntz et al., 2007). Unlike the majority of basaltic volcanism on the ESRP, the COTM lava field exhibits polygenetic volcanism (Hughes et al., 2002).

Lava flows found at the northern end of the Great Rift exhibit more evolved compositions, including trachybasalts, basaltic trachyandesites, and trachydacites (Hughes et al., 2019). As opposed to the monogenetic behavior typical of the older volcanism on the ESRP, these evolved compositions are found in conjunction with polygenetic eruption centers (Hughes et al., 1999). Both cinder cones and eruptive fissures are more common toward the northern end of the Great Rift (Kuntz, 1982), however, the origin of this relationship is debated. In comparison to the surrounding ESRP, the lava flows of COTM have higher Ti, Fe, Na, K, P, and lower amounts of Mg and Ca than the parent magmas, which suggests that contamination from the surrounding crust has occurred (Hughes et al., 1999; Stout et al., 1994). However, McCurry et al. (2008) have found that similarly evolved lavas located nearby can be explained through fractional crystallization of a parent magma consisting of basaltic trachyandesite, with <1% crustal contamination.

PROBLEMS WITH LAVA FLOW MORPHOLOGY TERMINOLOGY:

Understanding the processes that affect the morphology of lava flows and the current terminology is crucial to understanding the results of our study. The terms pāhoehoe and ‘a‘ā are Native Hawaiian words used to describe lava flows; these terms were first introduced into the scientific literature by Clarence Edward Dutton in 1883 (Harris et al., 2017). Although subsequent researchers have come to use these terms with regularity, a standard lexicon has yet to be fully established to this day. That is, a lava flow with slabs of broken crust has been called “slabby pāhoehoe” by some authors (Cashman et al., 1999; Duaiswami et al., 2002), but “slabby ‘a‘ā” by others (Lipman and Banks, 1987). Harris et al. (2017) recently tackled this terminology problem by proposing a classification system for lava flow textures that incorporates and standardizes the older terminologies. However, this system relies on field observations such as clast shape and vesicle type, and so is best suited for use by researchers in the field.

LAVA FLOW MOVEMENT AND INFLATION:

The most conceptually simple form of a lava flow is called pāhoehoe: most lava worldwide was emplaced as pāhoehoe (Self et al., 1998). Pāhoehoe typically moves in thin sheets or bulbous lobes. The outer surface of these sheets or lobes cools quickly, trapping molten lava beneath the cooled crust; as lava continues to flow into the molten interior from upstream, the outer cooled crust is lifted up (Hon et al., 1994.) This process is called inflation. If a lobe undergoes enough inflation, flow lobe tumuli can form; if a sheet undergoes enough inflation, it can become a lava rise (Rossi, 1996). The outer crust can also be pulled along in the flow and compressed, creating small-scale compression folds and giving that morphology the name “ropey pāhoehoe” (Figure 1).

Figure 1: Ropey pāhoehoe in Hawaii occurs when the cooling surficial "skin" of the flow is distorted by lava moving underneath it. Note the cm-scale arcuate compression folds.

DISRUPTED TEXTURES:

Rougher textures can form through a variety of means. Increasing either the shear strain or the viscosity of the lava will cause a transition from pāhoehoe to a disrupted texture such as ʻaʻā. One way disrupted textures can form is through crystallization, either due to cooling or to degassing. Degassing during magma ascent can produce more crystal-rich lavas, which

increases the viscosity and the yield strength of the resulting lavas and creates rougher textures both at the vent and downflow (Guilbaud, 2007). Cashman et al. (1999) found that smooth pāhoehoe forms when yield strength and crystallinity are low, and the crustal stability is high; as yield strength or crystallinity increases, the crustal stability decreases, thus forming disrupted textures. They suggest that a flow's primary texture is determined fairly shortly after the eruption, since the formation of a congealed crust traps heat and allows slow cooling, whereas disruption of the crust allows for rapid cooling and crystallization (Cashman et al., 1999; Sehlke et al., 2014).

Other researchers have noted that a lava flow's effusion rate, either from the vent or from an area of local storage, can cause disrupted textures. Rowland et al. (1990) found that high flow rates lead to ʻaʻā and other disrupted textures. Since high flow rates are typically the result of high effusion rates, this implies that lava flow textures reflect the eruption characteristics. However, disrupted textures have also been found downstream of areas of local storage (Duaiswami et al., 2002; Guilbaud et al., 2005; Keszthelyi et al., 2004).

LAVA FLOW MORPHOLOGIES:

SMOOTH PĀHOEHOE: Smooth pāhoehoe (Figure 2) is found as either small sheet flows or within channels (Self, 1998). No pāhoehoe flow is perfectly smooth; some amount of surface roughness always exists, but in relation to other lava flow morphologies, the surface roughness is very small. These flows are frequently found near vents or where the flow has a high effusion rate (Harris, 2017), but still has a low yield strength (Hon, 1994). Sheet flows are typically emplaced on slopes less than 2° (Hon, 1994). Lava channels tend to form during eruptions that are longer in duration as activity at the vent localizes into point sources (Self, 1998).

Figure 2: Smooth pāhoehoe in the foreground, showing cm-scale layers. Source: USGS Hawaii Volcano Observatory, 03/08/2012

LOBATE PĀHOEHOE: As the surface of the lava flow cools, a thin crust forms. After the crust has reached 2–5 cm in thickness, molten lava is trapped beneath it, creating submeter-scale bulbous ellipsoidal lobes connected by roughly cylindrical pathways of molten lava. Since there is a core of molten lava connecting these lobes beneath the cooled crust, the continued flow of lava can be accommodated by uplift of the crust and inflation of the lava flow (Hon, 1994). The individual lobes of pāhoehoe are inflated less than those in hummocky pāhoehoe (Figure 3).

Figure 3: Lobate pāhoehoe in Hawaii. Note the decimeter scale of the surface roughness.

HUMMOCKY PĀHOEHOE: Hummocky pāhoehoe (Figure 4) forms when inflation continues beyond the lobate scale: the individual lobes of pāhoehoe are hydrostatically connected by internal pathways of molten lava, and thus they inflate to the same height (Hon, 1994). Inflated flows frequently have monoclines, inflation clefts, and lava-rise pits (Walker et al., 1991; Harris et al., 2017). In our field area, the scale of the hummocky pāhoehoe was approximately 1 – 5 meters.

Figure 4: Hummocky pāhoehoe at COTM. Note the meter scale inflation features.

SLABBY PĀHOEHOE: Peterson and Tilling (1980) described slabby pāhoehoe as a transitional texture between smooth pāhoehoe and ‘a‘ā, with slabs of cooled pāhoehoe crust floating atop the lava flow, becoming jumbled and disoriented (Figure 5). Duaiswami et al. (2002) observed a flow toe that underwent inflation and cooling, allowing crystals to form in the molten interior, followed by an infiltration of molten lava underneath the crust that then broke out of the toe with a high strain rate and a disrupted texture. Harris et al. (2017) note that the slabs of crust can become imbricated and are often found on the surface of ‘a‘ā flows if the slabs are generated upstream of a transition to ‘a‘ā. Slabs can range in width from tens of centimeters to several meters across, with a thickness of several centimeters.

Figure 5: Slabby pāhoehoe at COTM. Slabby pāhoehoe is found in the middle ground and background. Note that the large boulders in the foreground are likely rafted agglutinate.

RUBBLY PĀHOEHOE: Keszthelyi et al. (2004) and Guilbaud et al. (2005) saw that an area of rubbly pāhoehoe formed when a lava flow underwent a pattern of stagnation that allowed a crust to form, followed by inflation, and then renewed movement that disrupted the crust, repeatedly breaking it into blocks and allowing molten lava to reach the surface (Figure 6). Rubbly pāhoehoe (Figure 7) is characterized by up to 50 cm wide and 2 m across with scraped grooves where they detached from the molten interior (Guilbaud et al., 2005; Harris et al., 2017). Slabs of pāhoehoe crust can be located near ridges in the flow (Keszthelyi et al., 2004).

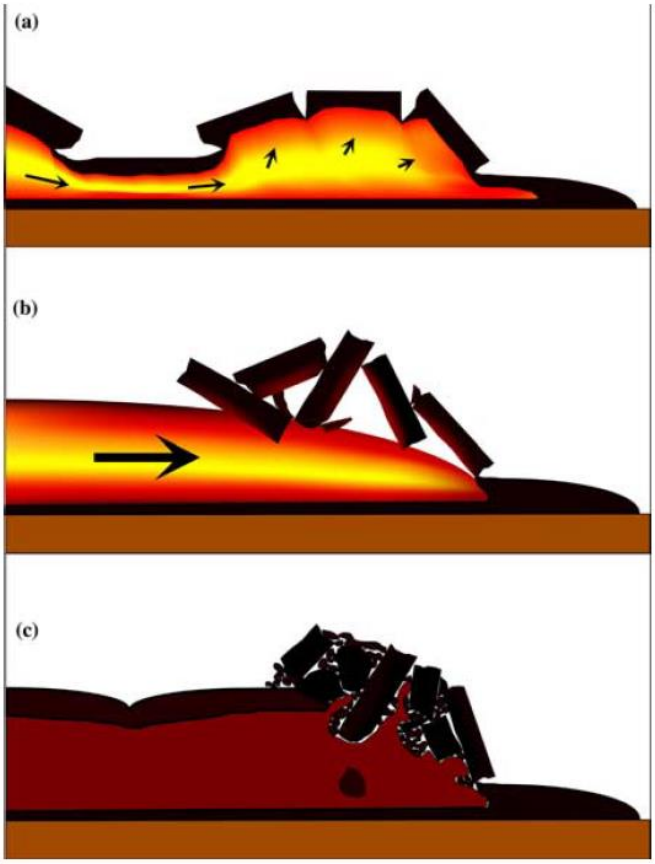

Figure 6: The formation of rubbly pāhoehoe as outlined in Keszthelyi et al. (2004): (a) inflation of a lava surface, (b) an influx of molten lava breaks apart the crust and compresses it, (c) molten lava intrudes into the overlying breccia. (Source: Figure 18, Keszthelyi et al., 2004).

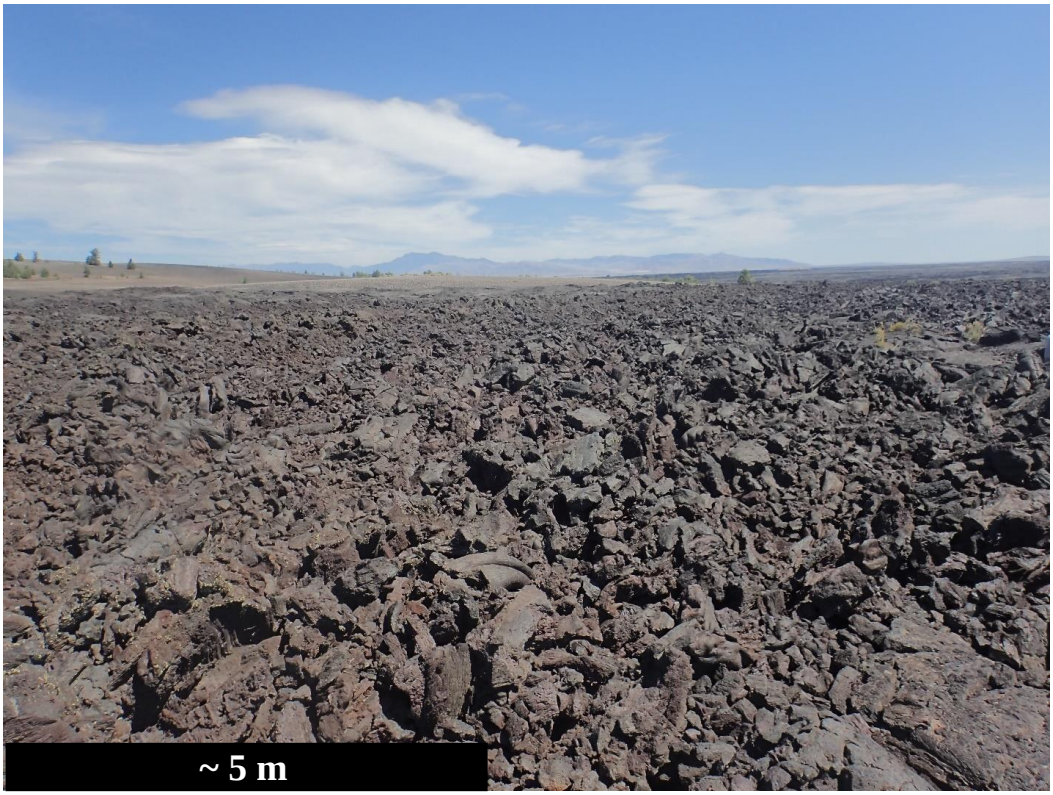

Figure 7: Rubbly pāhoehoe at COTM.

‘A‘ā: ‘A‘ā (Figure 8) forms when there is an increase in either the shear strain or the apparent viscosity [the ratio of total shear stress to the rate of shear strain (Peterson and Tilling, 1980)]. ‘A‘ā flows have an autobrecciated crust and base (Harris et al., 2017); as the flow advances, it drags the outer crust down beneath the flow front. ‘A‘ā flows have sub-rounded, jagged clinkers that can be as wide as tens of centimeters (Harris et al., 2017) and can be vesicular and jagged, denser and more rounded, or blocky and closer to equant (Lipman and Banks, 1987). The outer clasts that make up the autobrecciated crust are not attached to the flow interior. ‘A‘ā flows can also have lava balls that have been coated in multiple layers of accreted molten lava (Harris et al., 2017).

Figure 8: Lava flows in Hawaii, with an ʻaʻā flow texture on the left side and a pāhoehoe flow texture on the right side for comparison. Note that the molten interior of the flow is dragging down and rolling over the autobrecciated top crust. (Source: USGS Hawaii Volcano Observatory, 01/10/2013.)

BLOCKY-ʼAʻĀ HIGH RELIEF (HR): Blocky-ʼaʻā HR, a morphology we observed at COTM and informally named given the poor fit from existing nomenclature, has a jagged morphology with decameter-scale cracks, pits, and jagged spires, and meter-scale blocks (Figure 9). This rough morphology is probably due to the higher silica content of its lava (trachydacite, Hughes et al., 2019). Between the larger blocks, there is a second population of roughly equant blocks and jagged clinkers that can be tens of centimeters in width.

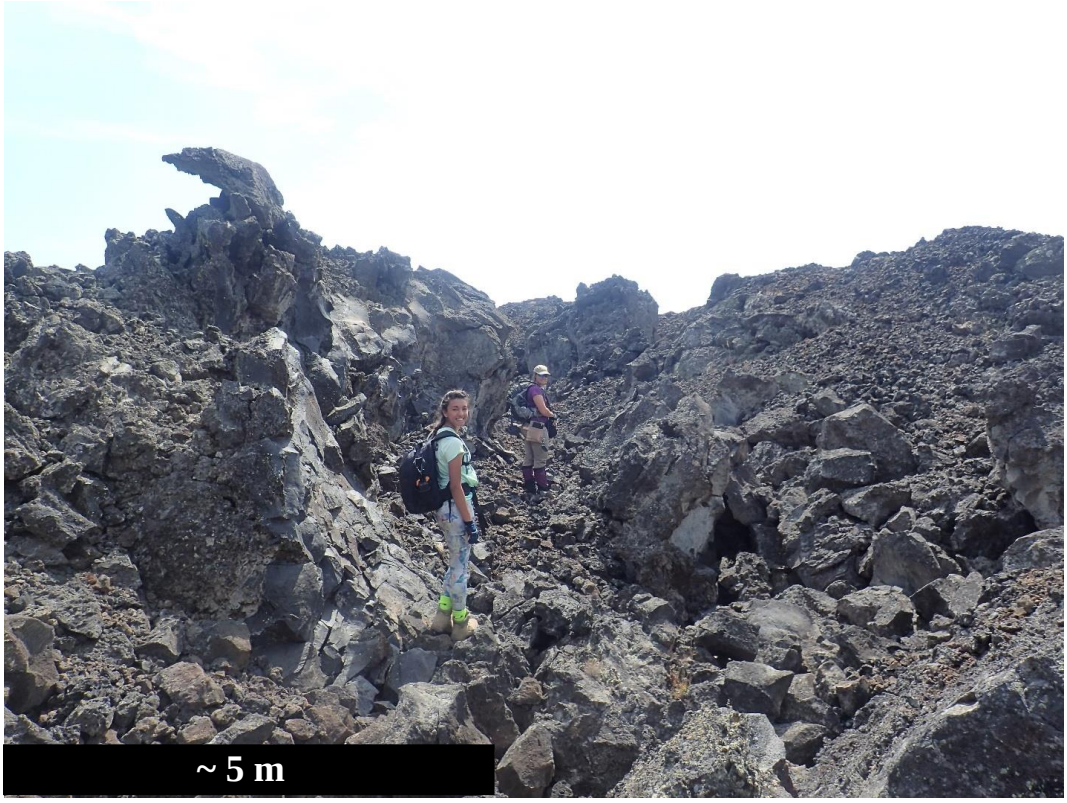

Figure 9: Blocky-'a'ā HR at COTM. Note the wide variety of clast sizes and shapes.

BLOCKY-'A'Ā LOW RELIEF (LR): This texture is also one that we identified in the field at COTM and tentatively named. It is characterized by centimeter to decimeter scale uneven and jagged clasts, with 1 – 5 meter scale blocks, pits, and extension cracks (Figure 10). This texture is found concurrent with blocky-'a'ā HR, however the predominately small clasts create a lower relief surface than that of blocky-'a'ā HR.

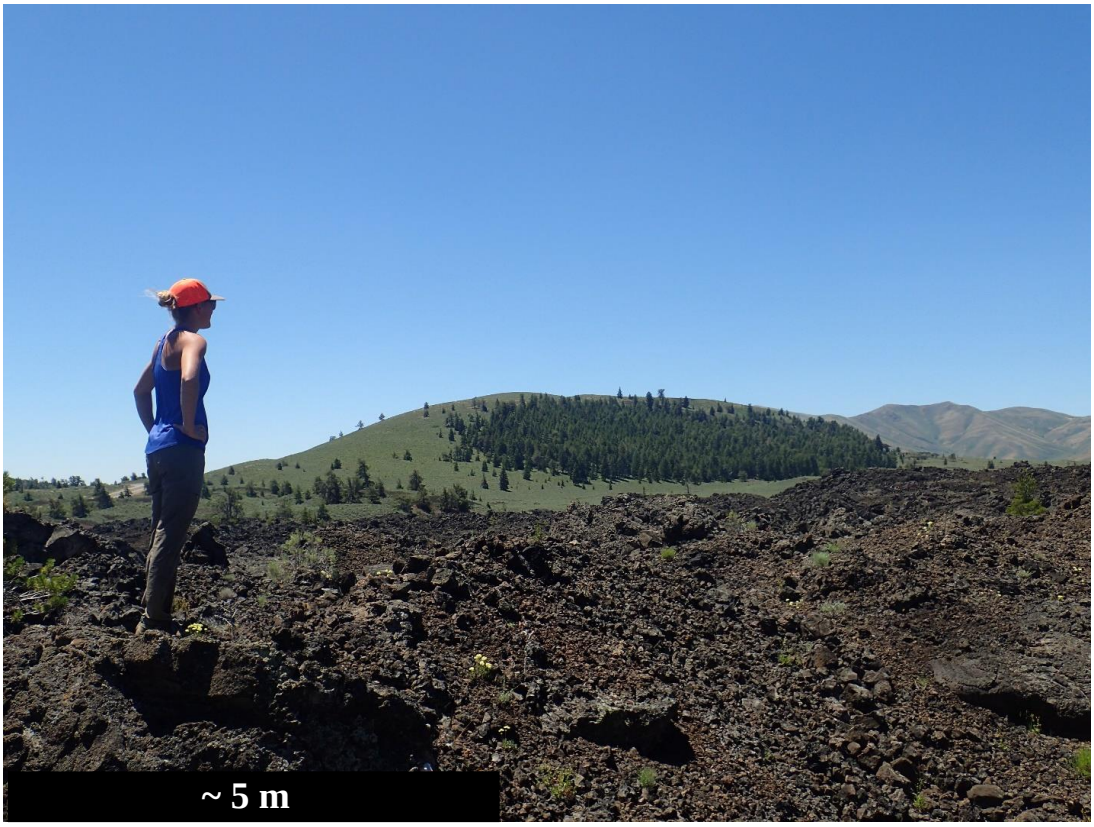

Figure 10: Blocky-'a'ā LR at COTM. Note the presence of meter-scale blocks that distinguish this texture from 'a'ā.

RUBBLY INFLATED PĀHOEHOE: Rubbly inflated pāhoehoe (Figure 11) is a hybrid morphology. It has small, almost equant blocks with occasional crustal pieces, consistent in size and shape with rubbly pāhoehoe. However, it also contains hummocks similar to hummocky pāhoehoe. Based on these factors, we think that this area formed first as rubbly pāhoehoe and then experienced inflation. Note that this, like the preceding two morphologies (blocky-'a'ā LR and blocky-'a'ā HR), is derived from our own field observations that did not cleanly fit within existing morphology types outlined in the literature (ex. Harris et al., 2017).

Figure 11: Rubbly inflated pāhoehoe at COTM. Note that from ground-level this morphology consists of cm to decimeter blocks and appears almost identical to rubbly pāhoehoe; walking out into the area immediately highlights that the rubble is actually arranged in waves approximately 2m in amplitude.

DATA COLLECTION AND PROCESSING USING STRUCTURE-FROM-MOTION:

Structure-from-motion (SfM) is a technique that combines overlapping photographs to create a three-dimensional model (Westoby, 2012.) One frequent application of SfM is the creation of Digital Surface Models (DSMs) using aerial images captured from UAS, kites, or airplanes (Smith et al., 2016). SfM is an inexpensive and efficient method that is becoming more widely used in the geosciences (Fonstad et al., 2013; Westoby, 2012). Our flight areas were selected to include a variety of lava flow textures, and the size of each flight area was based on estimated UAS flight time available given the conditions, payload, and battery. The majority of flights were conducted by Michael Downs of Kennedy Space Center with a Phantom quadcopter at heights ranging between 26 m and 92 m. Imagery was captured with a DJI FC330 digital camera (with a focal length of 4 mm, a resolution of 12.4 Megapixels, and an

image size of 4000 x 3000.) One flight area was selected and planned by the author and was flown by Dr. Donna Delparte of Idaho State University with a Steadidrone Hexcopter at a height of 50 m and a speed of 5 m/s. Imagery was captured with an Olympus E-PL5 digital camera (using a pancake lens with a focal length of 14 mm, a resolution of 15 Megapixels, an image size of 4640 x 3473, with a 75% side and forward image overlap.) The GPS on board the UAS was a VMAP survey grade device, and ground control points were surveyed with GPS. Flights were conducted at Craters of the Moon under research permit No. CRMO-2014-SCI-0004 during 2015 – 2016.

While initial SfM rasters had resolutions as high as 1 cm/pixel, it was necessary to degrade the DTMs into a series of consistent resolutions. We chose 0.1, 0.5, 1, and 2 m/pixel to span a range of resolutions, from that currently available from Mars satellites at the coarse end to aspirational views that are more consistent with LiDAR datasets.

STATISTICAL METHODS TO QUANTIFY ROUGHNESS AND GROUP SAMPLE AREAS:

Two methods were used to quantify roughness of the sample areas: RMS height and Area Ratio (Figure 12). Both approaches were applied as moving window calculations over the DTM rasters for each of the data resolutions considered in this study. The resulting rasters were combined to create two-band rasters for each resolution, with kmeans clustering used to identify roughness groups.

THE RMS HEIGHT:

The root-mean-square (RMS) height is commonly used to measure the surface roughness of terrestrial and planetary surfaces. The RMS height is a measure of the standard deviation of height about the mean, as given by the following equation:

$$\xi = \left[\frac{1}{n-1} \sum_{i=1}^{n} \left(z(x_i) - \bar{z} \right)^2 \right]^{1/2} \quad (1)$$

where ξ is the RMS height, *n* is the number of samples, z is the height, and x is the horizontal position (Shepard et al., 2001). Shepard et al. (2001) suggested that it be included as a standard method of measuring roughness, along with the RMS deviation or slope, the Hurst exponent, and the uncertainty in height measurements. Campbell et al. (1996) suggested that it be a standard measurement of roughness when coupled with the Hurst exponent. It has been used to analyze the roughness of the Moon (Cai et al., 2020), Mars (Garvin et al., 1999), and lava flows on Earth (Neish et al., 2016; Dierking, 1999).

Using the RMS height alongside the Hurst exponent is recommended by several authors (Campbell et al., 1996; Shepard et al., 2001). However, it was not feasible to do that in this work. The Hurst exponent describes the scalability of a two-dimensional surface using fractal characteristics. While it would be possible to calculate a series of Hurst exponents using parallel lines across a study area, this fails to account for the directional anisotropy of the surfaces of the lava morphologies. A three-dimensional version of the Hurst exponent has not yet been developed and therefore it would be inappropriate to use it in our three-dimensional study.

THE AREA RATIO:

The Area Ratio is the ratio of the two-dimensional planar area to the three-dimensional surface area (Grohmann, 2011), and is frequently referred to as rugosity. It is not used as commonly for lava flows, but it has been used on analyses of the roughness of coral reef systems (Duvall, 2018; Leon, 2015). The Area Ratio is described as:

$$R = \frac{\sum_{i=1}^{N-1} \sqrt{\Delta b_i^2 + \Delta x^2}}{(N-1)\Delta x} = \frac{1}{(N-1)} \sum_{i=1}^{N-1} \sqrt{1 + \left(\frac{\Delta b_i}{\Delta x}\right)^2}, \tag{2}$$

where R is the area ratio (or rugosity), x is the horizontal position, and b is the local gradient (Duvall, 2018).

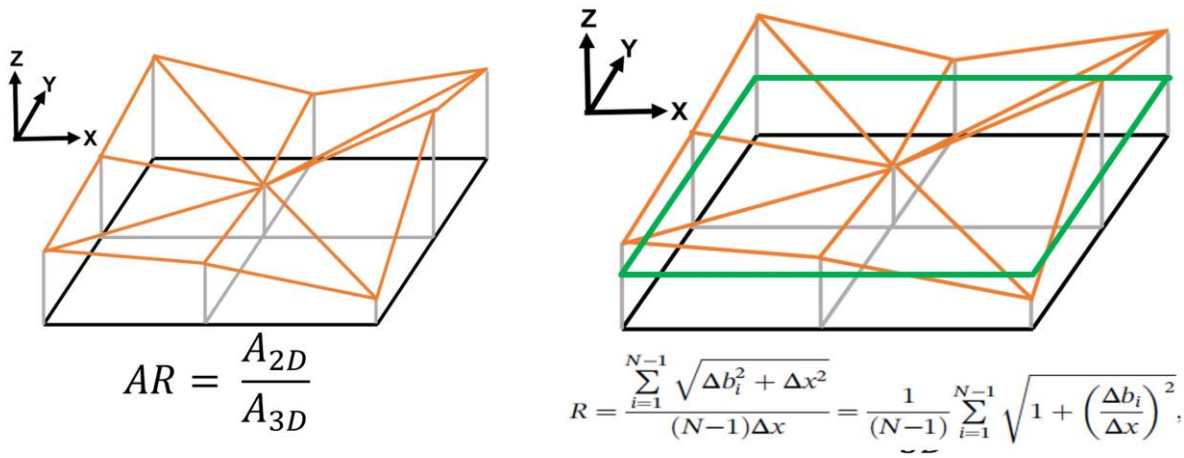

Figure 12 Illustration of the AR (a) and the RMS height (b) for a 3 pixel x 3 pixel moving window. Black is the two-dimensional map area, orange is the three-dimensional surface, and blue is the mean of the surface elevations.

THE KMEANS: The kmeans method places data into groups based on the least within-cluster sum of squares (WSS) between the data point and the centroid of the group: a data point is more likely to be placed into a group if it has a lower WSS between it and the group centroid (Steinley et al., 2006). It has been used to analyze topographic surfaces including the ocean floor (Lemenkova, 2019).

The RMS height and Area Ratio results for each sample area were combined into a 2-band raster for each of the data resolutions under investigation. The results were sorted into 100 evenly spaced bins across a range of 0 – 0.5 for the RMS Height and 0.7 – 1 for the Area Ratio. These ranges were chosen to highlight the ranges where the results showed the most variation;

the binned values within these ranges were combined into single dataset for each sample area, and these datasets were analyzed using the kmeans technique.

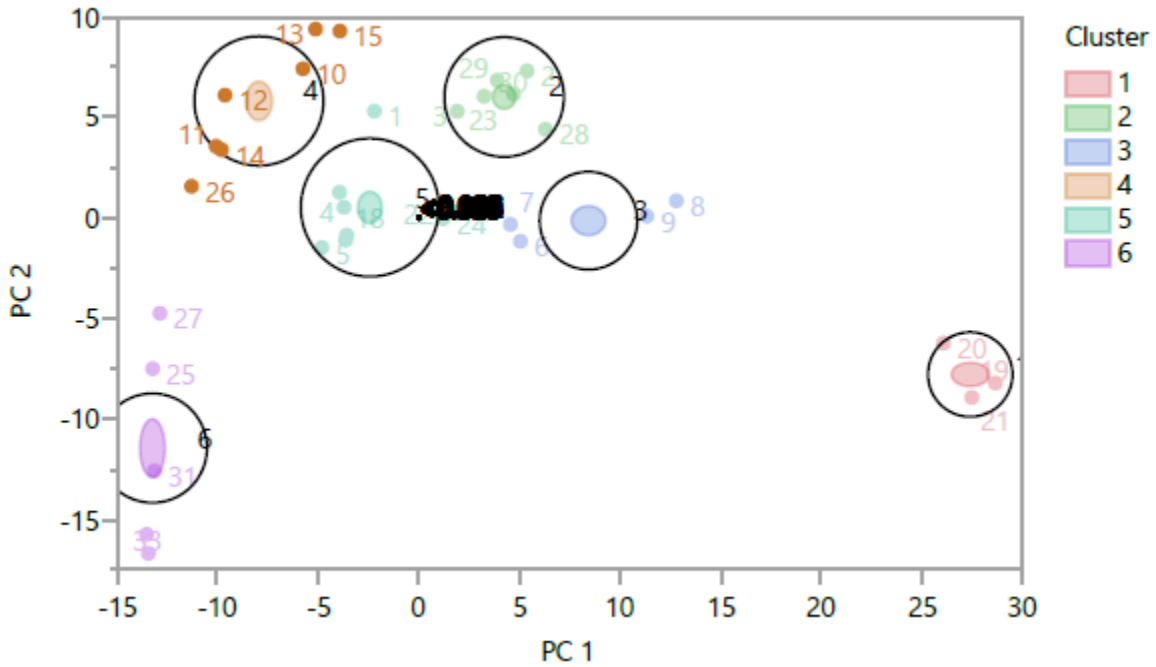

Figure 13: A plot of the clusters and centroids generated by analyzing the 0.5 m/pixel data using the 1.5 m x 1.5 m moving window.

ELBOW METHOD AND SILHOUETTE PLOTS

The kmeans method generates two types of plots: elbow and silhouette. The elbow plot shows the average distance to the centroid versus the number of groups. The ideal number of groups is indicated where the total within-cluster sum of squares between group sizes ceases to decrease significantly and begins to flatten, forming the "elbow" of the plot (Figure 13a).

The silhouette plot shows the cluster's silhouette width versus the number of groups (Figure 13b). The silhouette width is a coefficient that compares how similar a sample is to others of its cluster and how dissimilar it is from other clusters (Rousseeuw, 1986.) The peak of the graph indicates the ideal number of clusters.

We created both elbow plots and silhouette plots for the clusters generated by our kmeans analysis (Figure 14). These two plots were compared to find the ideal number of clusters for our analysis.

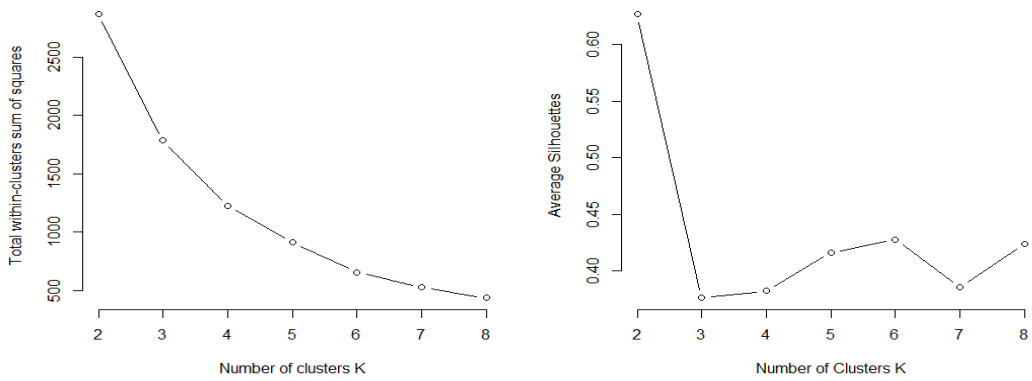

Figure 14: The elbow plot (left) and silhouette plot (right) for the 50 cm data resolution and the 1.5 m x 1.5 m moving window. Note the subtle inflection point at 6 clusters in the elbow plot and the peak at 6 clusters in the silhouette plot. This suggests that the ideal number of clusters is 6.

CHAPTER THREE: MANUSCRIPT FOR JOURNAL SUBMISSION

INTRODUCTION:

Lava flow morphologies are the result of conditions within the flow and external conditions affecting the flow during emplacement (Cashman et al., 1999; Hon et al., 1994; Guilbaud et al., 2007; Rowland et al., 1990; Self et al., 1998). There have been significant efforts to define lava flow morphologies and standardize their classification (Gregg et al., 2017; Harris et al., 2017; Hon et al., 1994; Keszthelyi et al., 2004; Lipman and Banks, 1987; Macdonald et al., 1953; Peterson and Tilling, 1980; Rowland and Walker, 1987). However, qualitative observations can be biased by unconscious factors, and variation in classification and terminology between observers continue to provide a challenge to standardization. In response, we propose here a classification tool based on quantitative descriptions of the lava flow surface roughness.

The classification of lava flow morphologies is more challenging in remote areas, including flows on other planets. Researchers have used several different techniques to address this problem, primarily using two-dimensional profiles (Cai et al., 2020; Kreslavsky, 2000; Lescinsky et al., 2006; Lipkaman et al., 2003; Rosenburg et al., 2011). Many authors combine several two-dimensional profiles or use a bidirectional statistic to better characterize the three-dimensional surface of a lava flow (Cai et al., 2020; Morris et al., 2008; Neish et al., 2017), however a three-dimensional analysis generates a more inherently robust description of roughness, especially for anisotropic surfaces. Thus, researchers are also developing methods of measuring roughness in three-dimensions using techniques such as the RMS Height (Cai et al., 2020), the topographic position index (Aufaristama et al., 2020), the improved morphological surface roughness (Cao and Cai, 2018), the wavelet leaders method (Deliege et al., 2017), and a

combination of homogeneity and entropy (Whelley et al., 2017). Here, we combine RMS height with Area Ratio, also known as rugosity, to quantitatively describe lava roughness. In both two-dimensional and three-dimensional studies, a relationship between the scale of geologic features and the scale of the surface roughness has been found, which can aid in feature identification (Cai et al., 2020, Garvin et al., 1999; Rosenburg et al., 2011; Whelley et al., 2017).

We used sample areas from the Craters of the Moon (COTM) National Monument and Preserve lava field in southeast Idaho, USA. We selected a terrestrial analog so that we could collect exceptionally high-resolution topographic data and downsample it to examine the impact of data resolution on lava morphology classification. We downsampled the data to two baseline high resolutions (0.1 m/pixel, 0.5 m/pixel) as well as resolutions consistent with the 1 m/pixel High Resolution Imaging Science Experiment (HiRISE) imagery of Mars (Kirk et al., 2008) and the 2 – 5 m/pixel Lunar Reconnaissance Orbiter Camera (LROC) imagery (Henriksen et al., 2017). It should be noted, however, that the scale of topographic features is very different on other planetary bodies, and so our numeric results are not directly transferable. Our classification method, however, is transferable to planetary surfaces (Shields et al., personal communication). Our method allows for a quantitative classification of lava flow morphologies, allowing for more consistency and reproducibility of interpretations between observers.

BACKGROUND:

FIELD AREA:

The Craters of the Moon (COTM) lava field is located in the eastern Snake River Plain (ESRP) in Idaho, United States. The ESRP is a 250 km long arcuate plain composed primarily of tholeiitic basalts and is oriented southwest-northeast (Kuntz, 1982). The COTM lava field is

composed of 1650 km^2 of Holocene lava flows that were erupted during eight eruptive cycles over the last 15,000 years along an 85 km long zone of crustal weakness called the Great Rift (Kuntz et al., 1982). The lava flows of the COTM field have higher amounts of trace elements than the olivine tholeiites that make up most of the ESRP and range in composition from tholeiitic basalts to trachydacites; this makes them more chemically evolved than other flows found in the ESRP and suggests the incorporation of crustal material (Hughes, 1999) or fractional crystallization (McCurry et al., 2008), which may contribute to the wide variety of lava flow textures found within the lava field (Neish et al., 2017). Previous researchers have described the surface morphologies as smooth pāhoehoe, hummocky pāhoehoe, slabby pāhoehoe, ‘a‘ā, and block lava (e.g., Kuntz, 2007; Geologic Resources Inventory, 2015; Tolometti et al., 2020).

The ESRP is the type locality for plains-style volcanism, a type of volcanism characterized by voluminous lava flows, containing lava tubes and channels, that are fed by point sources, shield volcanoes, eruptive fissures, and rift zones (Greeley, 1982). Similar plains volcanism has been identified on Mars (Greeley and Spudis, 1981; Hauber et al., 2009). Additionally, the ESRP, including COTM, has been used in a wide variety of planetary analog studies. While some studies have focused on the geochemistry (Hughes et al., 2019), petrology (Richardson et al., 2012; Adcock et al., 2018), or subsurface lava tubes (Garry et al., 2017; McHenry et al., 2010), others have considered the surface roughness (Neish et al., 2017; Tolometti et al., 2020).

COMMON LAVA FLOW MORPHOLOGY CLASSIFICATIONS:

Across the globe, many different lava flow morphologies have been identified (e.g., Harris et al., 2017). Here, we provide a list of the morphologies found in our field area (Figure 15), and briefly summarize their characteristic appearances as described by previous researchers.

Smooth pāhoehoe: Smooth pāhoehoe is characterized by a flat surface. Other than cooling cracks, smooth pāhoehoe exhibits little surface topography. This morphology is typically found as small sheet flows, within channels, or within lava ponds (Hon et al., 1994; Self et al., 1998). These small sheet flows can inflate as the surface of the flow cools quickly, trapping more molten lava beneath it (Peterson and Tilling, 1980).

Lobate pāhoehoe: Lobate pāhoehoe is characterized by decimeter to meter scale toes and lobes. These lobes form as molten lava breaks through the outer crust of the pāhoehoe; this breakout of molten lava can form a new lobe (Hon et al., 1994.)

Hummocky pāhoehoe: The hummocky pāhoehoe morphology has meter to five meter scale pits and plateaus. This morphology forms as the surface of the lava flow cools, trapping molten lava beneath a solidified crust (Hon, 1994; Walker, 2009.) As lava continues to flow, it intrudes beneath the surface curst, inflating the lava flow surface (Hon et al., 1994). This inflation process creates a lava morphology characterized by large flat plateaus, lava-rise pits, inflation ridges, inflation cracks, and tumuli (Walker, 2009; Rossi, 1996). The inflated surface may still have the remnants of the initial centimeter scale flow textures, however the flow as a whole has a much more rugged surface at coarser scales.

Slabby pāhoehoe: Slabby pāhoehoe is characterized by decimeter to meter scale slabs of smooth pāhoehoe crust that have been broken and rotated within the flow (Peterson and Tilling, 1980; Harris et al., 2017.) This disruption of the lava flow surface occurs due to changes in the

viscosity or shear strain present within a flow (MacDonald et al., 1953; Peterson and Tilling, 1980; Cashman et al., 1999; Rowland et al, 1990, Duaiswami et al., 2002).

Rubbly pāhoehoe: Rubbly pāhoehoe is characterized by decimeter scale, irregularly shaped blocks of lava, occasionally with scraped grooves (Harris et al., 2017). Occasional slabs of broken pāhoehoe crust are also found (Keszthelyi et al., 2004). This lava flow morphology is the result of disruption within the flow and is frequently found in locations that experienced changing effusion rates from the vent or local storage (Keszthelyi et al., 2004; Guilbaud et al., 2005.)

Blocky-'A'ā High Relief (HR): Blocky-'a'ā is the roughest of the lava flows in the COTM field and is considered our rough end-member morphology as no traditional 'a'ā was observed. This lava flow type is characterized by a rugged morphology with meter to decameter scale pits, extension cracks, and jagged spires. It must be noted that this morphology was observed specifically in the Highway Flow at COTM, which is a trachydacite rather than a basalt (Hughes et al., 2019).

UNUSUAL MORPHOLOGIES:

During the iterative process of developing our methods, two additional, non-standard morphologies came to light. Both structures were subtly distinct in aerial images but displayed unmistakable statistical differences in comparison to other similar morphologies. For the sake of clarity, we describe them here with the other morphologies instead of treating them as a later reveal in the results section.

Rubbly inflated pāhoehoe: The surface of this lava structure in the field has the small, irregularly shaped basaltic blocks characteristic of rubbly pāhoehoe while the broader topographic surface exhibited large ogives (compressional ridges) and hummocks consistent with

hummocky pāhoehoe. We interpret that this morphology formed first as rubbly pāhoehoe and then experienced inflation.

Blocky-'a'ā Low Relief (LR): In several places within the Highway flow (the trachydacite flow where blocky-'a'ā lava was observed) there are depressions filled with centimeter to meter scale clasts and meter scale blocks, pits, and extension cracks. These areas were broken out from the rougher sections of the Highway flow to avoid mixing the signals of these two morphologies.

SURFACE ROUGHNESS:

There are many ways to compute the roughness of a topography using two-dimensional profiles or three-dimensional surfaces. Some methods used to study profiles across lava flows are the RMS height (Campbell et al., 1996; Cai et al., 2020; Dierking et al., 1999; Garvin et al., 1999; Neish et al., 2016; Orosei et al., 2003; Shepard et al., 2001), RMS deviation, (Cai et al., 2020; Duvall et al., 2018; Morris et al., 2008; Shepard et al., 2001), Hurst exponent (Aufaristama et al., 2020; Cai et al., 2020; Morris et al., 2008; Neish et al., 2016; Rosenburg et al., 2011; Shepard et al., 2001), median absolute slope (Cai et al., 2020; Rosenburg et al., 2011), median differential slope (Kreslavsky et al., 2000; Rosenburg et al., 2011). These different metrics all attempt to address the same question: how can we quantitatively characterize flow roughness? Several studies have seen a correlation between an area's roughness and the scale of its features (Cai et al., 2020; Deliege et al., 2017; Kreslavsky et al., 2000; Lescinsky et al., 2006; Rosenburg et al., 2011).

However, lava flows are very anisotropic, and so using three-dimensional statistics gives a more complete characterization of the flow's morphology. Several different three-dimensional methods have been used to analyze the topography of lava flows, all of which have shown distinct differences in roughness between different lava flow morphologies. These three-

dimensional methods have included the RMS height (Cai et al., 2020); the topographic position index (Aufaristama et al., 2020), which compares the elevation at the center of a moving window to the average of the elevations within the window; the total curvature (Korzeniowska et al., 2018); and statistics that examine the randomness of roughness values (the entropy) and how smoothly the roughness changes within a certain region (the homogeneity, Whelley et al., 2014). These methods further our knowledge of three-dimensional roughness statistics that can be used for lava flow analysis, and we propose our method as a complementary method.

While a variety of techniques can be used to quantify surface roughness in two-dimensions, many of the more common techniques are quite complex to model in three-dimensions. For example, the Hurst exponent is commonly used to quantify the fractal nature of a topographic surface and one of the recommended techniques for quantifying roughness as described by Shepard et al. (2001); however, it is mathematically and computationally non-trivial to compute the Hurst exponent in three-dimensions, and at the present there is no universally accepted approach for handling the occurrence of anisotropic surface roughness for Hurst exponent calculations. Since lava flow morphologies can be strongly anisotropic, our goal was to analyze them using three-dimensional statistics.

Of these methods, this study focuses on the Area Ratio and the RMS height. These methods were selected because they are computationally straightforward to compute in three dimensions. We wrote two codes in Fortran 90 to perform these calculations using a user-defined moving window and skipping holes in the input data.

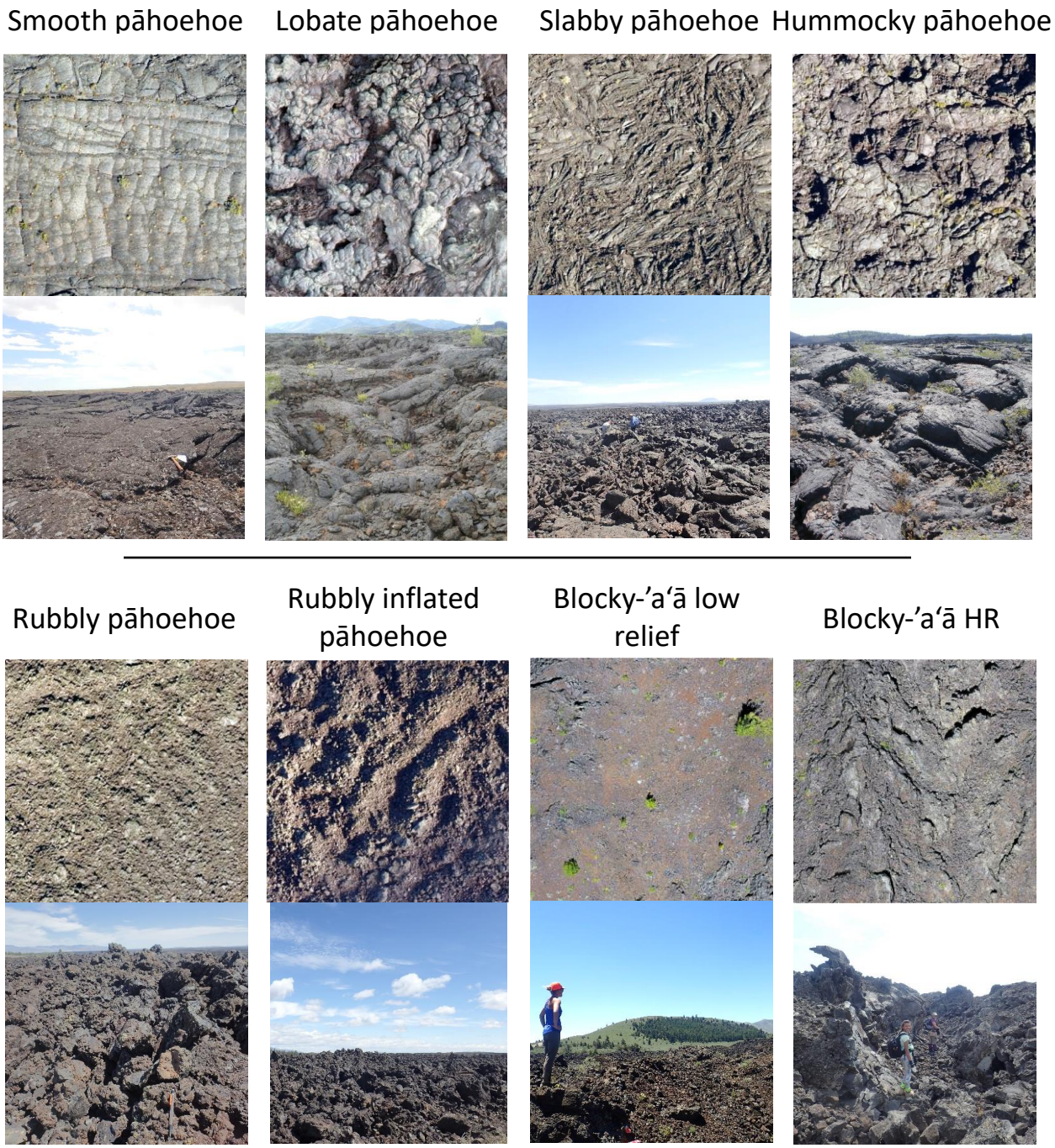

Figure 15: A priori lava flow morphologies as seen in aerial aerial images and in the field at COTM; note that the location of aerial imagery does not necessarily correspond to field photo.

METHODS:

DATA COLLECTION, PROCESSING, AND SELECTION OF SAMPLE AREAS:

Aerial images were collected using an Unmanned Aerial Vehicle (UAV) at the Craters of the Moon lava field (Figure 16) under research permit No. CRMO-2014-SCI-0004 during 2015 – 2016. Two sets of flights were conducted. The first set of flights was conducted with a Phantom 4 quadcopter flying at altitudes ranging between 26 m and 92 m. The camera on the Phantom quadcopter was a DJI FC330 digital camera with a focal length of 4 mm, a resolution of 12.4 Megapixels, and an image size of 4000 x 3000. The second set of flights was conducted with a Steadidrone Hexcopter at an altitude of 50 m and a speed of 5 m/s. The camera on the Steadidrone Hexcopter was an Olympus E-PL5 digital camera using a pancake lens with a focal length of 14 mm, a resolution of 15 Megapixels, an image size of 4640 x 3473, and 75% side and forward image overlap. The Steadidrone Hexcopter carried a VMAP survey grade GPS device, and ground control points were surveyed with GPS. Error report from the creation of orthophoto mosaics and DSMs is summarized in Table 1. Areas were selected based on in-situ and aerial imagery observations in order to include a diverse array of surface morphologies. In-situ classification included smooth pāhoehoe, slabby pāhoehoe, hummocky pāhoehoe, lobate pāhoehoe, rubbly pāhoehoe, blocky-’a‘ā (high relief), and blocky-’a‘ā (low relief). Given that this work is based on concerns with such subjective in-field classifications, these morphology names are provided as initial informative descriptions rather than as final designations.

Table 1 Errors reported during the DTM and orthophoto mosaic creation process.

Flight area	X error (m)	Y error (m)	Z error (m)
Big Craters Area 1	1.27323	0.773726	0.916356
Big Craters Area 2	1.41097	0.295218	1.30493
Big Craters Area 3	0.405066	1.5099	1.40154
Blue Dragon Area 1	1.04059	0.429358	1.78588
Blue Dragon Area 2	0.251107	1.33578	1.41679
Blue Dragon Area 3	0.9082	0.73415	1.25642
Highway	0.708987	1.33822	1.28794
North Crater Area 1	1.52327	0.206862	0.3268
North Crater Area 2	1.37955	0.132929	0.769363

The aerial images were used to create three-dimensional Digital Surface Models (DSMs) using the Structure-from-motion workflow (Westoby et al., 2012) in AgiSoft Photoscan. The original resolution of the DSMs varied from 0.01 m/pixel to 0.05 m/pixel. Square sample areas were clipped from these DSMs, with side lengths of approximately 40 m. Sample areas were placed to avoid textural changes or topographic anomalies. Due to the small size of the sample areas and the relatively flat regional slope, we did not detrend the data.

The bulk of the vegetation was identified using a trained maximum likelihood classification and the orthophoto mosaic. This vegetation was then clipped out of the DSMs, thus creating Digital Terrain Models (DTMs) of the sample areas. Any remaining large topographic irregularities (such as unusual holes or large trees missed by the initial trained classification) were manually removed. The sample areas were then downsampled using the Resample tool (bilinear interpolation) in ArcGIS to our chosen data resolutions: 0.1 m/pixel, 0.5 m/pixel, 1 m/pixel, and 2 m/pixel.

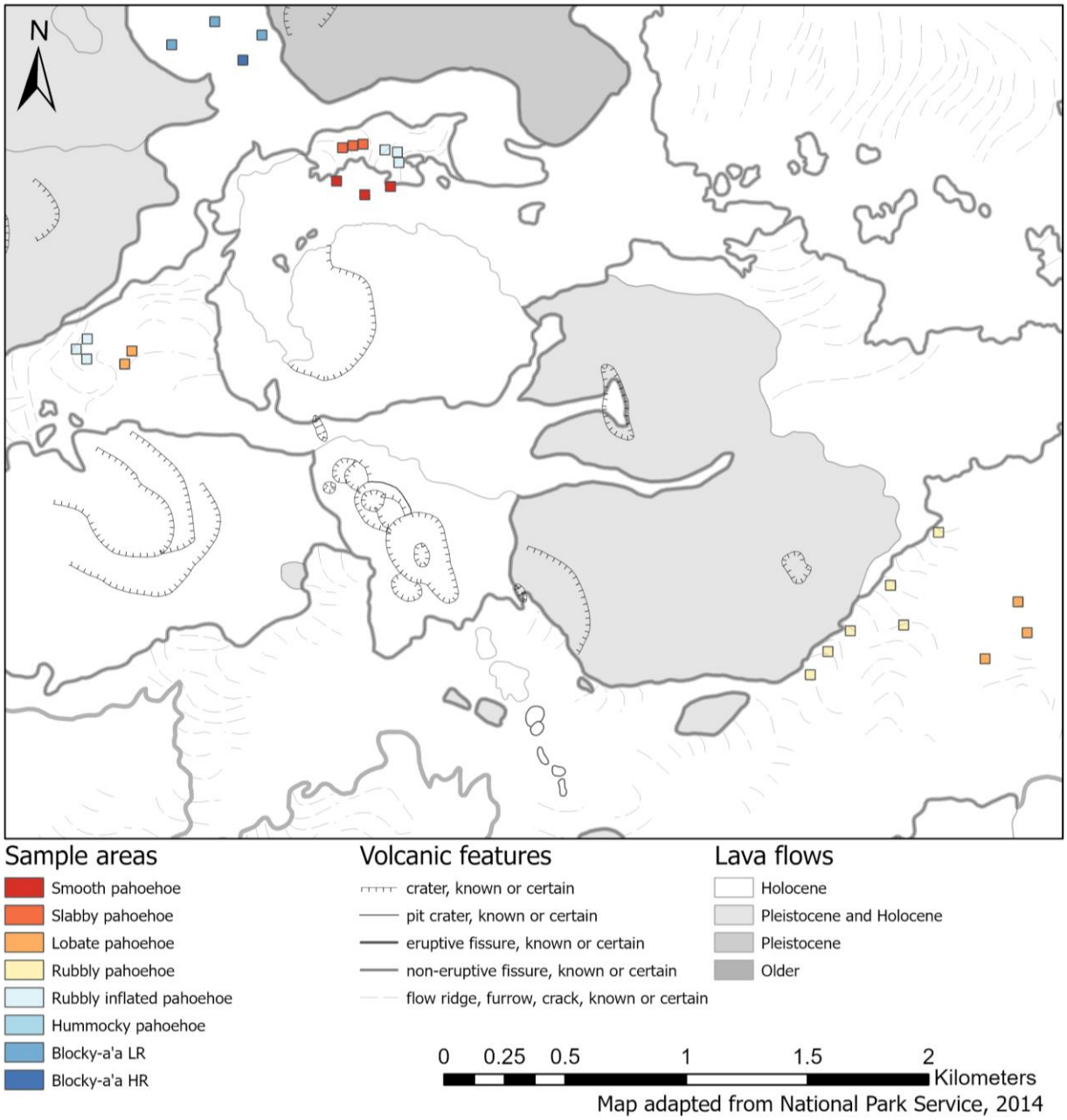

Figure 16: Location map of sample areas.

The devegetated holes were left empty in the 0.5 m/pixel, 1 m/pixel, and 2 m/pixel resolutions. Since we wanted to analyze the roughness of lava flows, we had the code skip areas containing holes within the moving window frame. There were many holes in the 0.1 m/pixel resolution, however, so skipping the holes prevented the code from generating results. Therefore,

we filled all the holes with the average of the surrounding pixels. The validity of this choice was tested in the 0.5 m/pixel resolution, for which we could compare calculation results from filled and unfilled vegetation holes; the impact that this had on roughness values is discussed in the results section of this paper. The downsampled and devegetated DTM rasters were exported as point data for use in the code.

MOVING WINDOW SIZES:

Two different moving window sizes were used to assess the topographic roughness. For both the Area Ratio and RMS Height techniques, the statistical analyses were computed over a 3x3 pixel window that scaled according to the data resolution. For example, the 0.1 m/pixel data resolution had a 0.3 m x 0.3 m moving window, while the 1 m/pixel data resolution had a 3 m x 3 m moving window. A 3x3 pixel moving window is common among studies of roughness (Grohmann et al., 2011).

We chose a ~7 m x ~7 m moving window as a larger moving window size to analyze all the data resolutions over a similar footprint size (0.1 m/pixel, 0.5 m/pixel, 1 m/pixel, 2 m/pixel). This size was motivated by the size of the 3x3 pixel footprint for the 2 m/pixel data; given that our approach requires an odd number of pixels on each side of the window in order to place the relevant calculation in the center pixel position of a given window position, we had to choose either a 5 m x 5 m or 7 m x 7 m window to accommodate the 1 m/pixel data. We selected the larger size option to ensure complete coverage relative to the corresponding 2 m/pixel window and adopted the same method of adding a single step in each direction to ensure an odd number of pixels per side for the finer data resolutions. As such, the actual window lengths were 7.1 m, 7.5 m, 7 m, and 6 m for the 0.1 m/pixel, 0.5 m/pixel, 1 m/pixel, 2 m/pixel datasets, respectively. Previous studies of roughness have found that different features are better differentiated with

different moving window or step sizes (Kreslavsky et al., 2000; Ozuomba et al., 2018; Whelley et al., 2017). Different window sizes were used to prioritize different scales of lava flow features: for example, a block that measures 3 m x 3 m x 3 m may look like an area of smooth pāhoehoe when analyzed with a 0.1 m x 0.1 m moving window, but will be identifiable as a large block when analyzed with a 7 m x 7 m moving window.

RMS HEIGHT METHOD:

The RMS height is the standard deviation of heights around the mean (Shepard et al., 2001) and is found using the following equation:

$$\xi = \left[\frac{1}{n-1}\sum_{i=1}^{n}(z(x_i) - \bar{z})^2\right]^{1/2} \qquad (1)$$

- where *n* is the number of points, *z* is the elevation, and z-bar is the mean elevation. Multiple studies have used the RMS height to classify topographic roughness, including Shepard et al. (2001), Orosei et al. (2002), Wu (2018), and Neish et al. (2017). It was suggested by Shepard et al. (2001) as one of the standard roughness metrics for natural surfaces.

AREA RATIO METHOD:

The Area Ratio (AR) is the two-dimensional planar area divided by the three-dimensional surface area (Grohmann et al., 2011). Values close to 1 are indicative of areas with a similar planar area and surface area, i.e., smooth areas. In comparison, values closer to 0.5 are indicative of rough surface areas. This method is also sometimes called rugosity (Leon et al., 2015). The three-dimensional surface area was calculated for each moving window via triangular planes defined by adjacent raster pixels, with the pixel value assigned to the central point of that pixel footprint.

CLUSTER ANALYSIS WITH THE KMEANS:

The kmeans method is an unsupervised machine learning technique that clusters data into groups by finding the least within-cluster sum of squares between the data point and the centroid of the group (Steinley et al., 2006.) Prior to using the kmeans method, we combined the Area Ratio and RMS Height results (Figure 17) for each sample area, and sorted these results into 100 bins of equal interval (ranging between 0.7 for the Area Ratio and 0 – 0.5 for the RMS Height. These ranges were selected because they had the most variability.) Combining the Area Ratio and RMS Height results allowed the kmeans method to use both those methods to determine the number of clusters present in our data. Using an unsupervised method allowed the model to disregard our a priori classifications and complete its analysis by focusing entirely on the quantitative roughness computed by our spatial metrics. This step is crucial in moving from a qualitative analysis to a quantitative analysis.

The results from the kmeans method were used to create elbow and silhouette plots that show the ideal number of clusters for each suite of conditions. The elbow plot graphs the number of clusters versus the average distance between the cluster centroid; the ideal number of groups is located where the distance decreases dramatically. The silhouette plot graphs the number of groups versus the cluster's silhouette width (a coefficient that compares the similarity between clusters.) The peak of the silhouette graph indicates the ideal number of clusters. We used both these types of plots in our analysis to choose the number of clusters for each combination of data resolution and moving window size.

RESULTS:

FILLED VERSUS UNFILLED DATA:

To evaluate the impact of filling in the holes and artificially smoothing the 0.1 m/pixel data, the 0.5 m dataset was processed using both filled and unfilled data. Analysis of the filled and unfilled 0.5 m/pixel DTMs for the same areas resulted in almost identical clusters. The largest difference was that the kmeans analysis on the unfilled data with the 7 m x 7 m moving window did not generate a cluster of slabby pāhoehoe. Thus, using the filled data for the 0.1 m/pixel data resolution may have generated somewhat different results than would have been generated with unfilled data, but we do not think that there was a notable difference to the clusters.

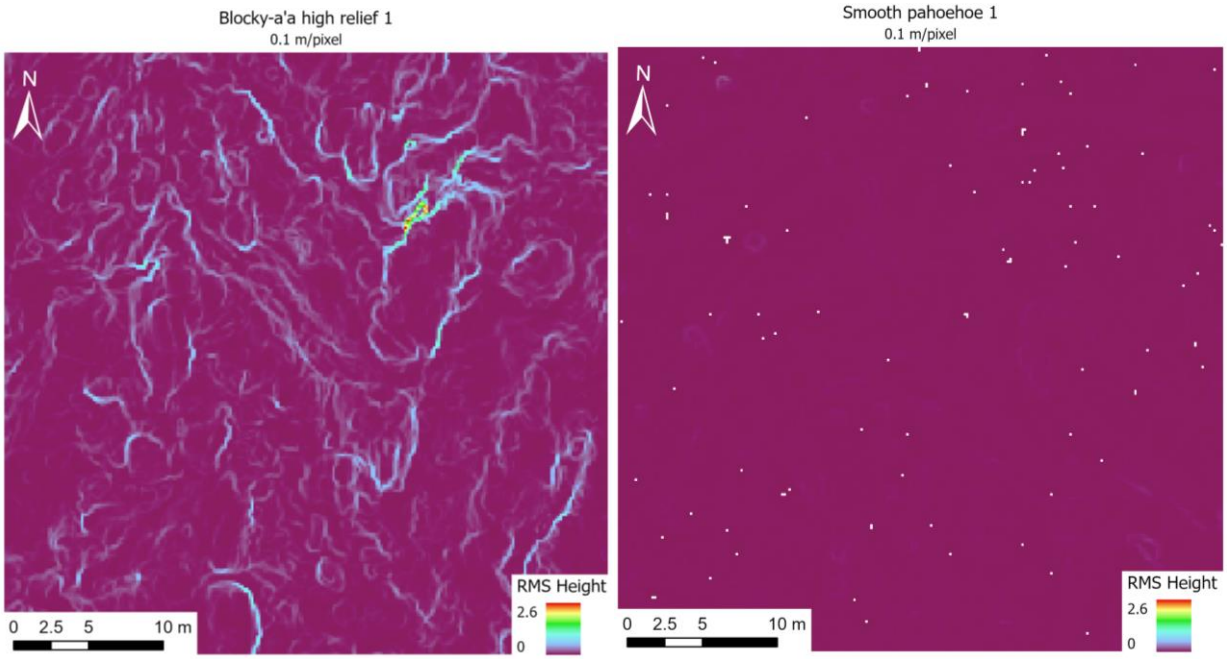

Figure 17 RMS Height results for an area of blocky-'a'ā HR and smooth pāhoehoe. Note that both sets of results are 0.1 m/pixel data, analyzed with a 0.3 m x 0.3 m moving window, and displayed using the same color ramp.

CLUSTERING RESULTS:

The sample areas clustered based on the scale of the roughness, which frequently correlated to field-based morphology observations (Table 2). While several of the a priori textures were grouped into clusters by themselves, other a priori textures varied between several clusters based on the number of clusters. In general, clusters included centimeter scale roughness (smooth pāhoehoe), centimeter to decimeter scale roughness (slabby pāhoehoe, lobate pāhoehoe, rubbly pāhoehoe), decimeter to meter scale roughness (lobate pāhoehoe, rubbly pāhoehoe, rubbly inflated pāhoehoe, blocky-’a‘ā LR), meter scale roughness (rubbly inflated, hummocky, blocky-’a‘ā LR), and decameter scale roughness (blocky-’a‘ā HR).

The various resolution and moving window size combinations grouped into either six or seven clusters. For groupings with the larger number of clusters, the seventh cluster split the small and medium scale roughness cluster into two.

Table 2: Cluster results found using the kmeans analysis. Each sample area is labelled with its a priori morphological classification. Note that the scale of roughness is a continuum.

Resolution (m) Moving window size (m) # of clusters	0.1 0.3 x 0.3 6	0.1 7 x 7 6	0.5 1.5 x 1.5 6	0.5 7 x 7 7	1 3 x 3 7	1 7 x 7 7	2 7 x 7 6
Scale of roughness Centimeter	Smooth1 Smooth2 Smooth3	Smooth1 Smooth2 Smooth3	Smooth1 Smooth2 Smooth3	Smooth1 Smooth2 Smooth3	Smooth1 Smooth2 Smooth3	Smooth1 Smooth2 Smooth3	Smooth1 Smooth2 Smooth3
							Slabby1
		Slabby1 Slabby3	Slabby1 Slabby3	Slabby1 Slabby3	Slabby1 Slabby3	Slabby1 Slabby2 Slabby3	
				Slabby2			
	Slabby1 Slabby2 Slabby3 Lobate1 Lobate2 Lobate3 Lobate4 Lobate5	Slabby2 Rubbly2 Rubbly3 Rubbly5	Lobate1 Lobate2 Lobate3 Lobate4 Lobate5 LR1 LR3	Rubbly2 Rubbly3 Rubbly5	Slabby2 Rubbly2 Rubbly3 Rubbly5	Lobate3 Lobate4 Rubbly4 Rubbly6	Slabby2 Slabby3 Rubbly2
Decimeter		Rubbly1 Rubbly4 Rubbly6 Lobate1 Lobate2 Lobate3 Lobate4 Lobate5 Rub-Inf1 LR3	Slabby2 Rubbly1 Rubbly2 Rubbly3 Rubbly4 Rubbly5 Rubbly6 Rub-Inf1	Lobate3 Lobate4 Lobate5 Lobate1 Lobate2 Rubbly1 Rubbly4 Rubbly6 Rub-Inf1 LR1 LR3	Lobate1 Lobate2 Lobate3 Lobate4 Lobate5 LR1 LR3	Lobate1 Lobate2 Lobate5 Rubbly1 Rub-Inf1 LR1 LR3	Lobate2 Rubbly1 Rubbly3 Rubbly5 LR3
Meter	Rubbly1 Rubbly2 Rubbly3 Rubbly4 Rubbly5 Rubbly6 Rub-Inf2 Hum3 Hum4 LR2				Rubbly1 Rubbly4 Rubbly6 Rub-Inf1	Rubbly3 Rubbly5 Rubbly2	Rubbly4 Rubbly6 Lobate1 Lobate3 Lobate4 Lobate5 Rub-Inf1 Rub-Inf3 Rub-Inf4 Rub-Inf6 LR1 LR2
1 - 5 meters	Rub-Inf1 Rub-Inf3 Rub-Inf4 Rub-Inf5 Rub-Inf6 Hum1 Hum2 LR1 LR3	Rub-Inf2 Rub-Inf3 Rub-Inf4 Rub-Inf5 Rub-Inf6 Hum1 Hum2 Hum3 Hum4 LR1 LR2	Rub-Inf2 Rub-Inf3 Rub-Inf4 Rub-Inf5 Rub-Inf6 Hum1 Hum2 Hum3 Hum4 LR2	Rub-Inf2 Rub-Inf3 Rub-Inf4 Rub-Inf5 Rub-Inf6 Hum1 Hum2 Hum4 LR2	Rub-Inf2 Rub-Inf3 Rub-Inf4 Rub-Inf5 Rub-Inf6 Hum1 Hum2 Hum3 Hum4 LR2	Rub-Inf4 Rub-Inf5 Rub-Inf6 Rub-Inf2 Rub-Inf3 Hum1 Hum2 Hum3 Hum4 LR2	Rub-Inf2 Rub-Inf5 Hum1 Hum2 Hum3 Hum4 HR2
Decameter	HR1 HR2 HR3	HR1 HR2 HR3	HR1 HR2 HR3	Hum3 HR1 HR2 HR3	HR1 HR2 HR3	HR1 HR2 HR3	HR1 HR3

IMPACT OF DTM RESOLUTION:

Smooth pāhoehoe is separated from other groups at the 0.1 m/pixel, 0.5 m/pixel, and 1 m/pixel resolution; at the 2 m/pixel resolution, the small amplitude group also contains an area of slabby pāhoehoe. Blocky-'a'ā HR was also separable at data resolutions lower than 2 m/pixel, but clustered with rubbly inflated, hummocky, and blocky-'a'ā HR when using the 2 m data resolution. This suggests that the 2 m data resolution is too coarse to distinguish the end-member textures from similar textures.

MOVING WINDOW SIZES:

Moving window size affects which textures are distinguished at which data resolutions. Sometimes, the difference between the two moving windows is minimal - for the 0.1 m/pixel data, the 7 m x 7 m moving window clustered slabby pāhoehoe and rubbly pāhoehoe, whereas the 0.3 m x 0.3 m moving window clustered slabby pāhoehoe and lobate pāhoehoe. In both of those cases, the features grouped with the slabby pāhoehoe had characteristic block scales on the decimeter scale. However, sometimes the difference between the two moving windows is more impactful. The ability of a moving window to distinguish textures is dependent on the scale of the textural features and the data resolution. For large morphologic features, a small moving window size might not be able to capture the entire relevant feature, providing instead a series of partial views. Similarly, a data resolution coarser than the characteristic scale of the features will result in smoothing of the DTM such that it becomes difficult to differentiate between morphologies characterized by finer roughness scales.

While one might initially hypothesize that the 0.1 m/pixel dataset viewed through the 7 x 7 m moving window would provide the best results by combining the data resolution with the largest moving window, it did not significantly outperform the other combinations under

consideration. We hypothesize that this is because the scale of many textures was significantly larger than the data resolution.

DISTINGUISHABLE MORPHOLOGIES:

Areas classified a priori as slabby pāhoehoe was differentiated in the following combinations: 0.1 m data resolution with a 7 m x 7 m moving window, 0.5 m/pixel data resolution with both moving window sizes, and the 1 m data resolution with both moving window sizes. While slabby and lobate pāhoehoe have similar scales of roughness, they have very distinct morphologies: lobate pāhoehoe is the original flow surface, whereas slabby pāhoehoe is the result of disruption and breaking of the original flow surface into large plates. These differences in morphology represent significant differences in flow history, and so it is valuable to be able to differentiate these textures from one another. Lobate pāhoehoe and slabby pāhoehoe were clustered together with the 0.1 m/pixel data resolution and the 0.3 x 0.3 m moving window. Lobate pāhoehoe could be isolated by subtracting areas of slabby pāhoehoe (identified using the data resolution and moving window combinations previously described) from the areas classified as slabby and lobate pāhoehoe using the 0.1 m/pixel data resolution and the 0.3 x 0.3 m moving window.

Rubbly inflated and hummocky pāhoehoe are always grouped together in our results. This could be due to the large amplitude and wavelength roughness of the hummocks and other inflation features overwhelming the smaller scale roughness from the actual rubble. We anticipate that these two units could be better differentiated from one another through the inclusion of a slope layer in the cluster analysis, providing more information about the structure of the roughness in the RMS height and Area Ratio layers.

Our Area Ratio-RMS height clustering method identified different scales of roughness that correlated with different lava morphologies. Unsurprisingly, end-member morphologies such as smooth pāhoehoe and blocky-'a'ā HR were easily distinguishable in all data resolutions. The roughness values for intermediate textures overlapped, which is logical because these textures grade into one another. Using a combination of analyses conducted at different data resolutions with different moving window sizes, several of the a priori intermediate textures were distinguishable; this is explored more in the Discussion section.

DISCUSSION:

STATISTICAL CLASSIFICATION OF TEXTURAL GROUPS VERSUS FIELD CLASSIFICATION:

While the model output classifications are not a perfect representation of our *a priori* classifications, it reflects generative processes like inflation and disruption. Specific combinations of data resolutions and moving window sizes could be selected to define specific morphologies for future analysis. For example, lobate pāhoehoe and slabby pāhoehoe are clustered together using the 0.1 m/pixel data resolution and 0.3 x 0.3 m moving window, as well as in the 0.5 m/pixel and the 2 m/pixel data resolutions with the 7 m x 7 m moving window. The 0.5 m/pixel and 1 m/pixel data resolutions placed slabby pāhoehoe into a group by itself. Thus, one could find the slabby pāhoehoe areas using the 0.5 m and 1 m data resolutions and subtract those areas from the 0.1 m small-amplitude group to isolate the areas of lobate pāhoehoe. Similarly, the slabby pāhoehoe areas identified in the 0.5 m/pixel and 1 m/pixel data resolutions could be used to extract areas of rubbly pāhoehoe. Some clusters contain only slabby pāhoehoe and rubbly pāhoehoe: the 0.1 m/pixel data resolution with the 7 m x 7 m moving window; the 0.5

m/pixel data resolution with the 1.5 m x 1.5 m moving window; the 1 m/pixel data resolution with the 3 m x 3 m moving window; and the 2 m data resolution.

One limitation to this work is the lack of ‘a‘ā in the study area. A key lava flow morphology for basalts, ‘a‘ā is frequently thought of as an end-member opposite smooth pāhoehoe. However, we posit that the roughness signature of ‘a‘ā will be fairly close to rubbly pāhoehoe, as they are close neighbors on the continuum of lava flow morphologies, especially when considering the scales of resolution considered in this work. Data collection on flows such as those in Hawaii would be necessary to incorporate this morphology.

An important aspect to note in our work was that we found morphologies not readily apparent in visual imagery. Rubbly-inflated was such a morphology. We initially classified these areas as rubbly pāhoehoe based on the clast sizes observed in aerial imagery, however the roughness signature proved to be very different. We examined the raster outputs of the Area Ratio and RMS Height (Figure 18) and noticed that the rubble in those areas were actually arranged in ogives, or a series of compressional ridges indicative of inflation. Given this observation, we broke these areas out into their own a priori group called rubbly-inflated. We decided to split these morphologies out into independent groups to examine the strength of our method regarding transitional morphologies, to support the notion that lava flow morphologies are not relegated to the few identified in the field by past researchers, and to support our position that objective observations can be supported by quantitative data analysis.

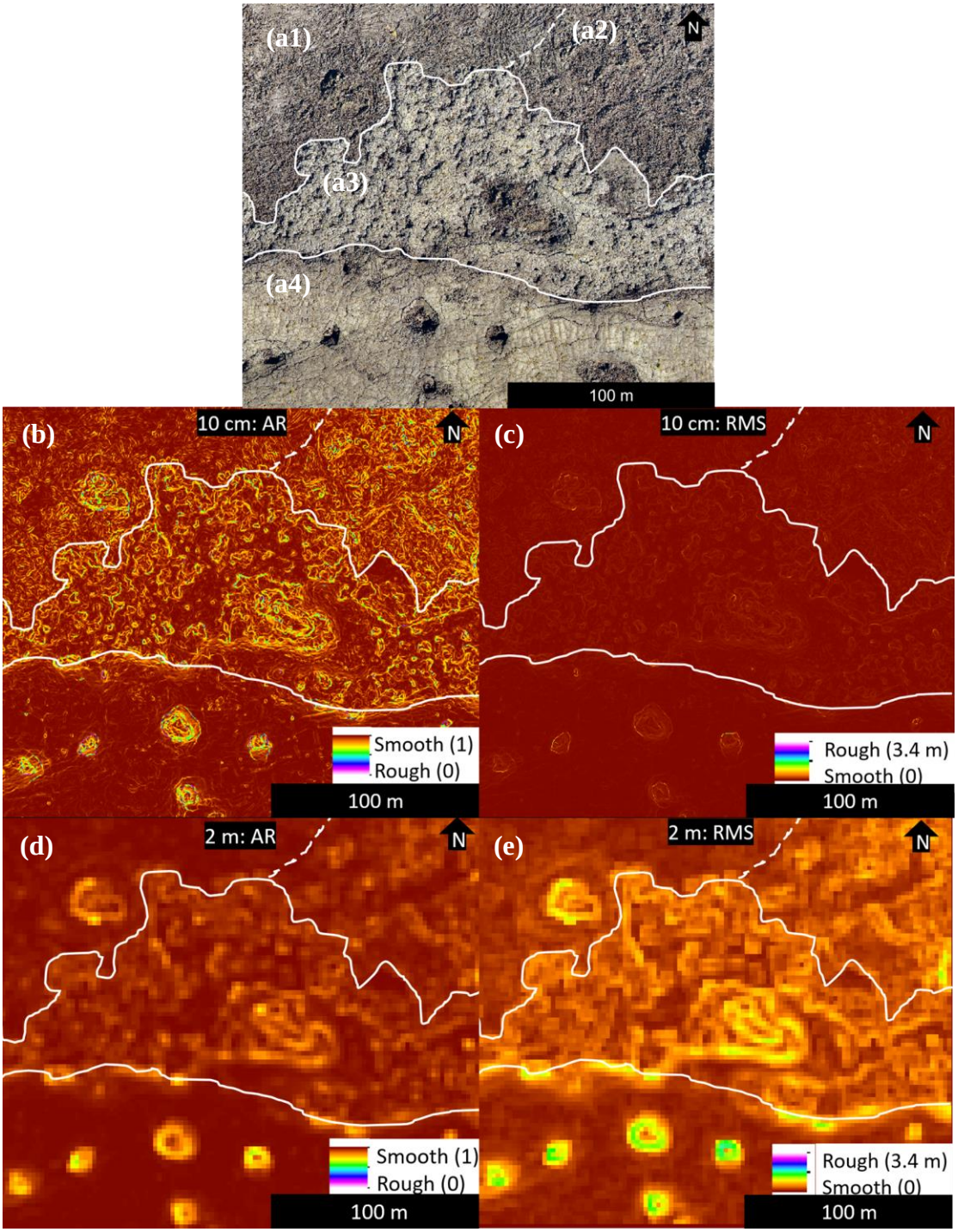

Figure 18 Lava flow morphologies as seen in the AR and RMS Height. (a) Visible imagery of (a1) rubbly pāhoehoe, (a2) rubbly-inflated pāhoehoe, (a3) hummocky pāhoehoe, and (a4) smooth pāhoehoe. (b-c) The AR and RMS Height results for the 0.1 m/pixel data resolution and the 0.3m x 0.3 m moving window. (d-e) The AR and RMS Height results for the 2 m/pixel data resolution and 7 m x 7 m moving window. Note that vegetation and large topographic anomalies have not yet been removed. The difference in roughness between rubbly pāhoehoe, rubbly-inflated pāhoehoe, and hummocky pāhoehoe is evident.

THE IMPACT OF DATA RESOLUTION ON TEXTURAL CLASSIFICATION:

While we performed our analysis at a high data resolution (0.1 m/pixel), we did not see a large difference in the clusters generated for the 0.1 m/pixel and the 0.5 m/pixel DTMs. A more refined classification of intermediate morphologies might be achievable either through incorporation of more roughness metrics in the kmeans clustering or through analysis of higher resolution DTMs, however, for most textural analyses, the 0.5 m/pixel data is likely sufficient. Any possible improvement from increased DTM resolution would need to be evaluated against the increased computational cost from the much larger data volume, as well as consideration of whether the means of data collection is actually producing reliable surface data at that higher resolution and for large enough areas to be useful.

We found that the driving factor in distinguishing flow textures was not merely the moving window size or the data resolution, but rather the combination of data resolution and moving window size. This is likely the result of different textural features being distinguished better at certain resolutions and window sizes: i.e., the slabs of slabby pāhoehoe are best picked up in the 0.5 m/pixel data resolution with the 1.5 x 1.5 m moving window because the slabs are meter scale. The 0.1 m data resolution is likely picking up the small-scale details on the surface of the pāhoehoe slabs; conversely, the 7 m x 7 m moving window is likely combining several individual meter-scale slabs. Our work provides useful guidance for future researchers looking to determine the data resolution and moving window sizes required for their work. For terrestrial studies, we recommend using data resolutions ranging from 0.5 m/pixel to 1 m/pixel. Our methods could still be used on 2 m/pixel data if budget or payload constraints dictated a lower resolution, however this would limit the differentiable textures to smooth pāhoehoe and blocky-

’a‘ā . We would recommend a scaling moving window (i.e., the 3x3 moving window) to differentiate intermediate morphologies.

IMPLICATIONS FOR THE MOON AND MARS:

These methods can be applied to terrestrial datasets as well as those from other planetary bodies; while the roughness values will be different due to the different conditions of the lava flows, precursor imagery will aid in selecting appropriate DTM resolution and moving window sizes. Cai et al. (2020) found that the RMS deviation (the RMS of the deviation of the actual values from the expected values) at small data resolutions was higher for martian lava flows than terrestrial flows and lower for lunar flows than terrestrial flows.

To capture those higher roughness values, we recommend using 1 m/pixel and 2 m/pixel data DTM resolutions (such as that from HiRISE) and a combination of a 3 m x 3 m and 7 m x 7 m moving window sizes in future studies of lunar and Martian lava flows. Larger moving window sizes could also be appropriate to match the scale of features on Martian flows. That would make it possible to distinguish a wide variety of textures, including smooth pāhoehoe and blocky-’a‘ā HR. Using combinations of data resolution and moving window size, other textures could be distinguished, possibly including hummocky pāhoehoe, rubbly pāhoehoe, slabby pāhoehoe. While our study did not include ‘a‘ā, we posit that ‘a‘ā could be distinguished using a combination of those data resolutions and moving window sizes.

One other significant factor when examining topographic features on the Moon and Mars with this method is the significant presence of dust and regolith. This fine sediment infills and obscures flow features, smoothing out the surface of the lava flow and making it more difficult to perform a statistical analysis of flow morphologies. This could be partially addressed by

classifying and removing areas of significant dust accumulation from the analyses. If the dust was small scale, then it could likely be isolated as a distinct texture and then removed. To better distinguish it from smooth pāhoehoe, we would recommend using 1 m or 2 m data resolutions. If aerial imagery were available, a trained classification could also be tried in an attempt to classify and remove dust accumulation.

FUTURE WORK:

In the future, other statistical methods of computing three-dimensional roughness could be included in the kmeans cluster analysis. These include methods that have previously been used for two-dimensional transects, like the Hurst exponent and the Allen deviance (Neish et al., 2017; Shepard et al., 2001) and three-dimensional methods such as the homogeneity, entropy (Whelley et al., 2017), and topographic position index (Aufuristama et al., 2020). We chose not to use these computationally intensive methods due to the scope of our work, however they could be combined with our methods to further refine the classification process, and possibly to better characterize intermediate morphologies. While looking at the clusters generated at different data resolutions allows us to consider the fractal scalability of our work, we did not generate meaningful results from using the kmeans technique on a combination of the RMS and AR results of all data resolutions. This was because the numerical values generated by the different window sizes and data resolutions created increased apparent overlap between the datasets as the kmeans was not successful in treating each distribution set as a distinct layer. We hypothesize that using a more sophisticated machine learning technique, such as a neural network, would address this problem. These techniques could also be used to classify and autonomously map lava flows that contain many textures. Additionally, since this set of methods distinguishes lava flows, any number of morphologies could be added, including ‘a‘ā. Adding morphologies could

help to identify other common morphologies, such as ‘a‘ā, or morphologies that have previously not been discussed, much like the rubbly-inflated found in our field area.

CONCLUSION:

Classifying lava flow morphologies is frequently subjective, especially when using remote sensing datasets. We analyzed the surface roughness of different lava flow morphologies using three-dimensional spatial statistics. Digital terrain models were downsampled to 0.1 m/pixel, 0.5 m/pixel, 1 m/pixel, and 2 m/pixel data. Roughness statistics included the Area Ratio and the RMS height and were calculated using both a scaled moving window (e.g., a window 3 x 3 pixels wide) and a set moving window (7 m x 7 m). We then separated our sample areas into clusters using the kmeans. The clusters generated by the kmeans frequently correlated with the a priori morphology classifications that were based on field observations. Individual a priori morphologies clustered differently based on the data resolution and moving window size; however, clusters tended to include centimeter scale roughness (smooth pāhoehoe), centimeter to decimeter scale roughness (slabby pāhoehoe, lobate pāhoehoe, rubbly pāhoehoe), decimeter to meter scale roughness (rubbly pāhoehoe, rubbly inflated pāhoehoe, blocky-’a‘ā LR), meter scale roughness (rubbly inflated pāhoehoe, hummocky pāhoehoe), and meter to decameter scale roughness (blocky-’a‘ā HR). We were also able to distinguish end-member morphologies (smooth pāhoehoe and blocky-’a‘ā HR) at all data resolutions and moving window sizes. This type of terrain analysis is a worthwhile application of relatively new technology (UAS), structure-from-motion, large data analysis, and machine learning techniques.

These methods of quantitative lava flow analysis allow us to objectively classify lava flow morphologies. Field methods have been instrumental in developing our knowledge of basaltic lava flow morphologies and mechanisms; however, there is an inherent subjectivity

present in observational data collection. Our classification method can be used to better understand and map flow morphology transitions and unusual flow morphologies, as we demonstrated in our analysis of rubbly inflated pāhoehoe. Additionally, our method could be used to map flow morphologies across inaccessible areas such as remote lava flows on Earth, or lava flows on other planets such as the Moon and Mars.

CHAPTER FOUR: DISCUSSION AND CONCLUSION

In this chapter, I will expand on the discussion section from the manuscript meant for submission to a journal (Chapter 3). In addition to what was already discussed, I investigated several other methodologies that were not continued. Some yielded inconclusive results, while others were promising and should be further investigated by others. I will also use this space to offer some more speculative suggestions for future data resolution goals for lunar and martian surface data in order to best facilitate orbital mapping and interpretation of those planetary bodies.

OTHER METHODS OF QUANTIFYING SURFACE ROUGHNESS:

While developing the method described in the paper above, we tried a variety of other methods, some of which were more successful than others. A brief discussion is included here.

We tried several pre-made roughness analysis tools that did not work well for our needs. One of these was TextureCam, a program primarily designed to analyze photographs taken with rovers and classify geologic features such as rocks and sediment (Wagstaff et al., 2013). Preliminary work has also shown this program to be effective at classifying ground versus cloud cover in orbital imagery (Thompson et al., 2013). However, we did not have good results when using this method on our aerial images (Figure 19). This method involves creating a file with different colored areas that correspond to different textures shown in a corresponding image (i.e., a training data set). Then the computer applies this training data to other images, and classifies the textures found in the other images. This tool can classify as many textures as the user wants, however we tested it with images containing only two textures. If further work was done to test this tool, we would recommend incorporating more training data.

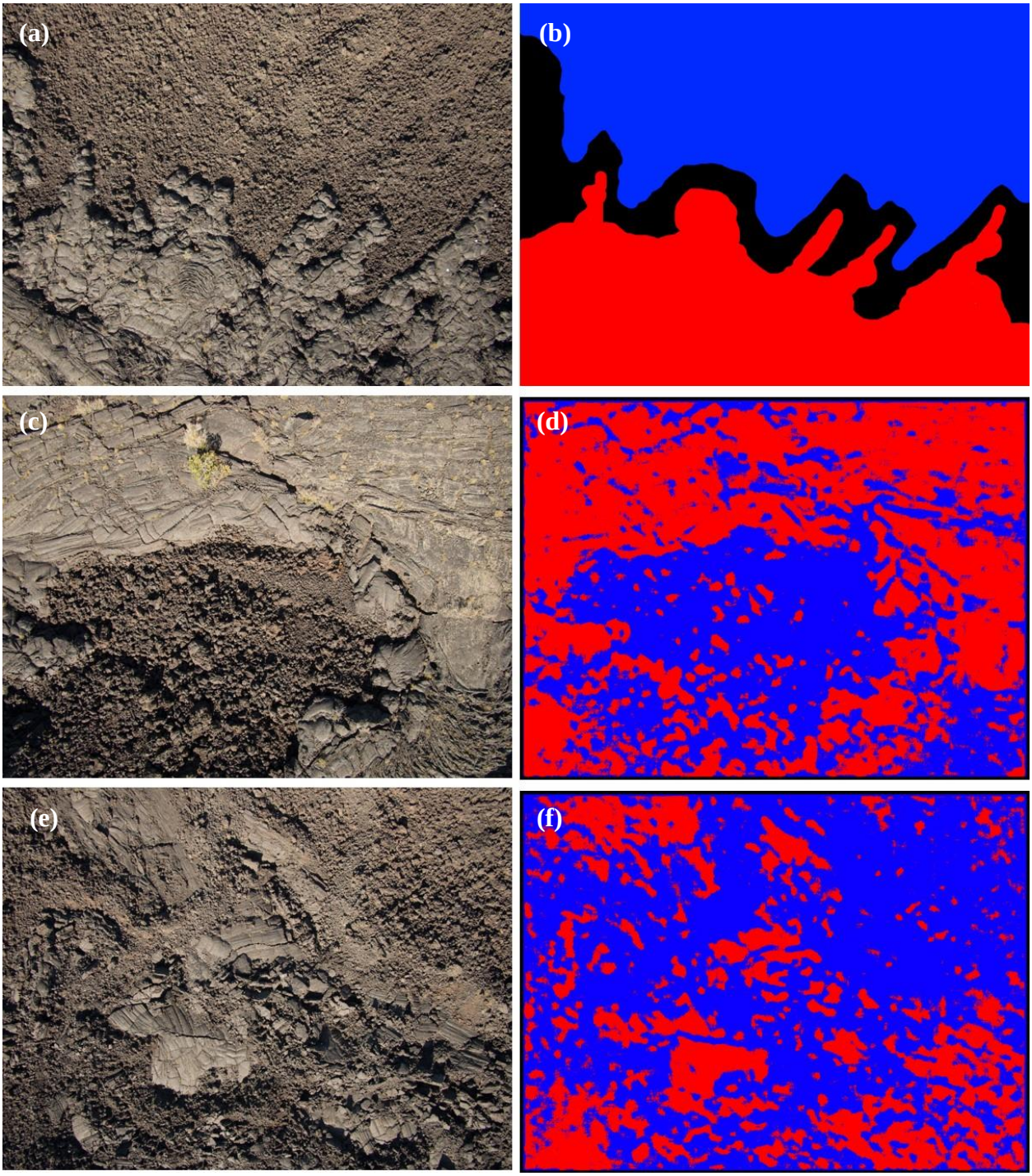

Figure 19: TextureCam test results. (a) Visual imagery for training and (b) training labels. Blue is rubbly pāhoehoe, red is another flow morphology, and black is no data. (c-f) Visual imagery for a classification test of two areas of rubbly pāhoehoe.

Another pre-made tool we tried was the Benthic Terrain Modeler, an ArcGIS toolbox designed to analyze and classify seafloor topography using several different statistical methods. One of these is the Terrain Ruggedness method which computes the Area Ratio (also known as the rugosity) (Grohmann et al., 2011). While this tool would have saved us a great deal of coding effort, the tool did not allow users to actively control the moving window size. Since multiple moving window sizes were an important aspect of our study, this meant that we were unable to fully utilize the Terrain Ruggedness method.

We also tried several of the basic focal statistic tools built into ArcGIS, such as Mean Value, Range of Value, and Standard Deviation, to analyze the DTMs. These methods distinguished between large and small amplitude roughness morphologies but did not distinguish medium-amplitude textures from large or small. These methods were not an improvement on the results we got from the RMS Height and Area Ratio methods and did not allow for the size of the moving window to be changed. The Curvature tool found similar results between all morphologies, and so was not included for further study.

The ArcGIS tool that did produce potentially useful results was the Slope tool. This tool generated a wide enough range of output for the various morphologies that we thought the Slope tool had a high likelihood of distinguishing flow textures. However, the ArcGIS method only allowed for a 3 x 3 pixel moving window, with no option to change the moving window size; this has since been upgraded in ArcPro 2.8, which was released after this portion of the study was completed. We encourage future researchers to use the new Slope tool in Arc or to write a code that will measure the slope angle and aspect using a planar best-fit across a variably-sized moving window. We anticipate that this would be particularly useful in order to differentiate

between relatively smooth slopes found on inflated pāhoehoe hummocks and the rougher slopes associated with rubbly-hummocky pāhoehoe.

Another commonly used tool within roughness analysis is the Hurst exponent, which is a means of calculating the fractal self-similarity of roughness across different scales (Turcotte, 1997). An example of fractal topography is a watershed: as you increase the scale of observation, the dendritic pattern changes scale but maintains its shape. Previously, Neish et al. (2016) used the Hurst exponent to describe linear transects of lava topography at COTM in order to compare with their radar-based roughness calculations. While they were successful in correlating the linear Hurst exponents with their raster data, the use of the linear Hurst exponent is very vulnerable to anisotropy in the measured surface. As such, orienting the measurement line parallel or perpendicular to flow direction may produce very different results. Recent attempts to get around this issue by combining Hurst exponent calculations from two perpendicular lines (Aufaristama et al.; 2020Cai et al., 2020) remain vulnerable to the orientation of those lines relative to anisotropic morphologic features. Work by Rosenburg et al. (2011) to formulate a radial algorithm for the Hurst exponent has not been broadly adopted, and programming it from scratch was beyond the scope of this work. We did attempt to write a Fortran 90 code for a middle-ground approach that would calculate the Hurst exponent for four crossing lines (north-south, east-west, NE-SW, NW-SE) at each pixel to create four separate raster maps that could be combined as CYMK heatmaps, thereby preserving visual information about the degree of fractal self-similarity as a function of orientation. While the north-south and east-west Hurst exponent calculations for a given pixel were relatively easy to achieve, more high performance computing expertise is necessary to properly manage the memory issues that emerge from trying to calculate the Hurst exponent on the diagonals for relatively large datasets (McGregor, personal

communication). We remain very interested in the possibilities for this code to be developed in the future and applied to lava terrain analysis.

We gained a great deal amount of insight into the validity of our methods by examining the standard deviations of both the RMS height and Area Ratio results (Figure 20). The standard deviations show differences between some of the transitional textures, such as between hummocky-rubbly and hummocky (Figure 19). Future work on this project could add the standard deviation of the RMS and AR results to the kmeans analysis to better define transitional morphologies.

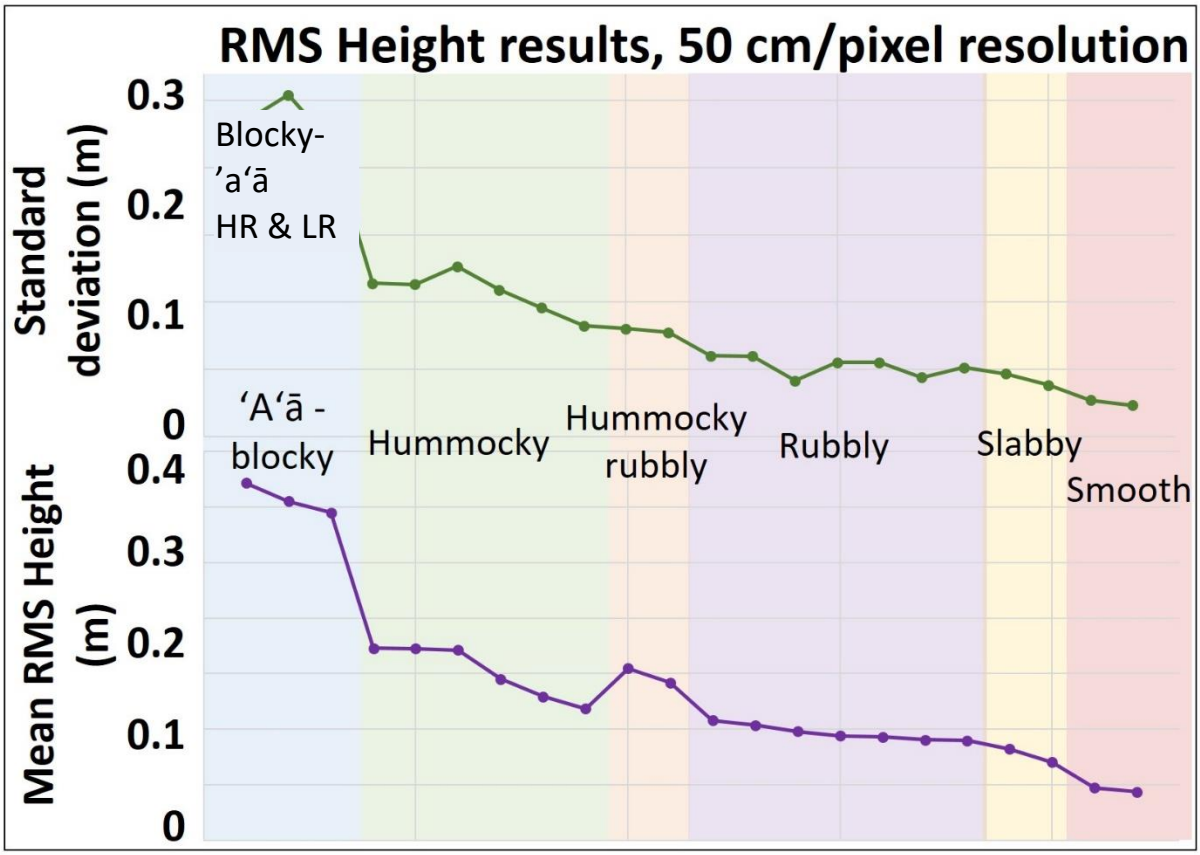

Figure 20: The mean RMS height and standard deviation results for the 0.5 m/pixel data resolution. Note that each point corresponds to a data set assigned that a priori morphology.

In addition to the kmeans, we tried doing a hierarchical cluster analysis with dendrograms (Figure 21). The dendrogram method creates clusters by minimizing the Euclidean distance between data points. The agglomerative method used by R iteratively combines the closest data points into nodes. In R, the dendrogram method results in a tree-diagram: each node breaks apart into several branches, and the closer the branches are, the more similar the datasets are. Each color represents a group, with the number of groups specified by the user. This was very helpful for understanding the clustering and generated very visually attractive results; however, we chose to use the kmeans method because the kernel function that JMP uses for the kmeans tool distinguished the lava flow morphologies slightly better.

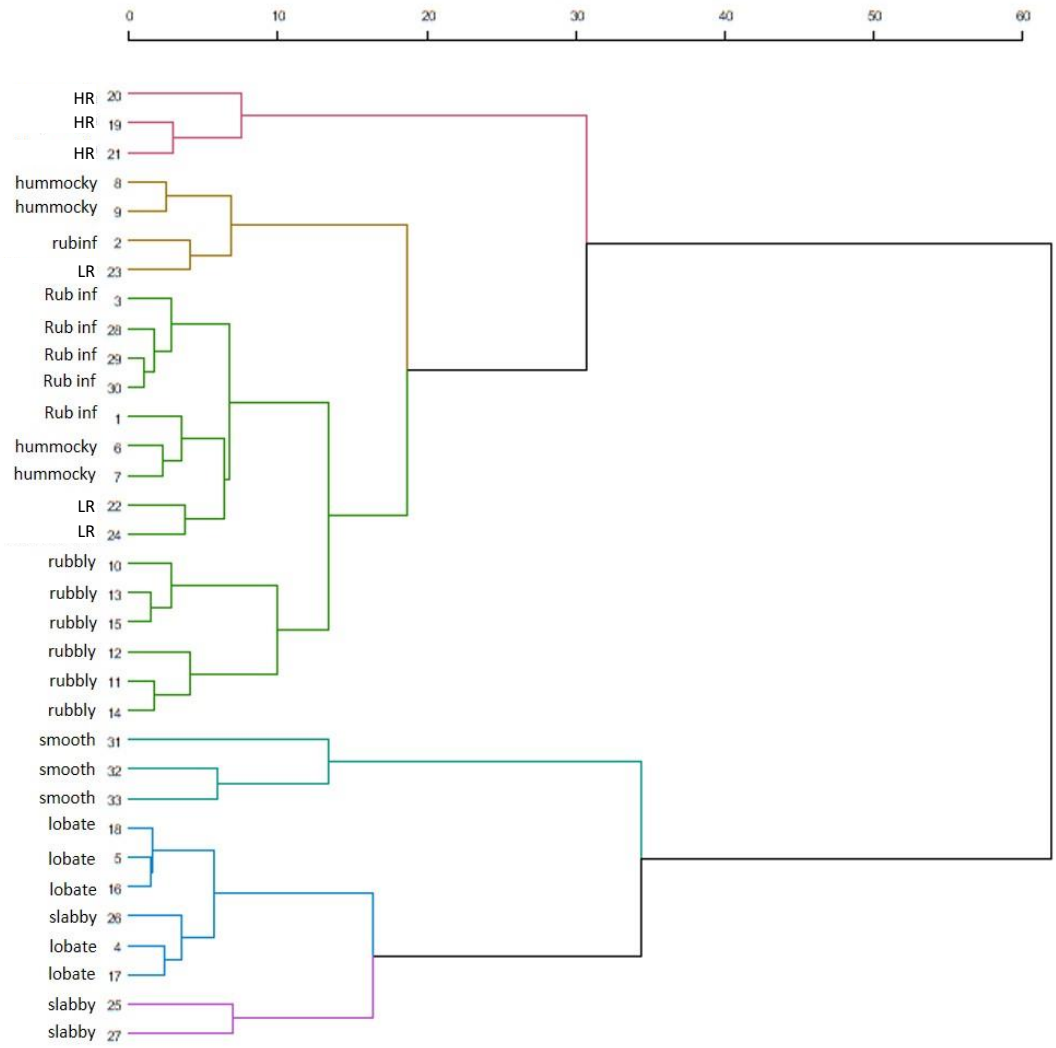

Figure 21: The dendrogram results for the 10 cm data resolution and a 3 x 3 moving window.

FUTURE WORK:

Future work should include the slope, as described earlier, and may also benefit from the inclusion of the standard deviation of the slope. Our preliminary tests of the built-in ArcGIS slope tool generated good results, but the median, differential, and RMS slope have been used by other researchers to good effect (Cai et al., 2017; Campbell et al., 1996; Grohmann et al., 2011; Neish et al., 2016; Shepard et al., 2001). This effort will require the development of a tool that

readily enables the user to control the size and positioning of the moving window to use when calculating the local slope.

While our comparison of analyses conducted on filled and unfilled 0.5 m/pixel DTMs indicated minimal change in classification outcome from filling the vegetation holes, future work should test that result for other data resolutions. Using filled data would make it easier to conduct some of the analyses that were not included in this research, such as the slope and Hurst exponent.

These methods could be expanded to create an automated mapping program that analyzed, clustered, and classified lava flow morphologies. Using that expanded methodology, entire lava flows could be mapped in a quantitative fashion. The clusters found in this analysis could also be corelated with petrologic analyses, which could then be used to infer the petrology of lava flows on other planets. This would give significant insight into the volcanic history of both terrestrial and planetary surfaces.

CONCLUSION:

Determining lava flow morphology is a fairly subjective process in the field based primarily on visual observations of surface slopes and clast shape and size. Efforts are being made to standardize these in-situ classifications (Harris et al., 2017), however identifying morphologies in satellite and aerial imagery still remains quite subjective. Most analyses rely on qualitative field observations (Harris et al., 2017; Lipman and Banks, 1987; Peterson and Tiling, 1980), and so it was our goal to develop a quantitative method of classifying lava flow morphologies.

Researchers have examined the roughness of terrestrial and planetary surfaces in a multitude of ways, however most work on lava flows have used two-dimensional methods. Some three-dimensional methods have been used, including the RMS height (Cai et al., 2020), the topographic position index (Aufaristama et al., 2020), the improved morphological surface roughness (Cao and Cai, 2018), and the wavelet leaders method (Deliege et al., 2017).

We used the RMS Height and the Area Ratio methods to quantify the roughness of lava flow morphologies in three-dimensions, and then used the kmeans hierarchical clustering method to determine what groups of morphologies were distinguishable in DTMs derived from high-resolution aerial images. We conducted this analysis for several different data resolutions (0.1 m/pixel, 0.5 m/pixel, 1 m/pixel, 2 m/pixel) and two styles of moving window: a 3 x 3 pixel moving window, and a 7 x 7 m moving window.

Using these methods, we were able to group areas based on the scale of their roughness. These groups frequently corresponded to our a priori morphological classifications. At the 0.1 m/pixel and 0.5 m/pixel data resolutions, smooth pāhoehoe, blocky-’a‘ā HR, and several intermediate textures were distinguishable. At the 1 m/pixel and 2 m/pixel data resolutions, smooth pāhoehoe and blocky-’a‘ā HR were distinguishable. By using a combination of data resolutions, other morphologies could be distinguished such as lobate pāhoehoe, slabby pāhoehoe, and rubbly pāhoehoe.

This method can be used to analyze imagery from terrestrial flows and those on other planets. For terrestrial flows, this method can help standardize lava flow morphology classification, particularly for flows in remote locations. For flows on other planets, this method can aid with flow morphology identification, mapping, and the analysis of volcanic history. This method could also be useful in planning landing sites.

WORKS CITED

Adcock, C. T., Udry, A., Hausrath, E. M., Tschauner, O., 2018. Craters of the Moon National Monument basalts as unshocked compositional and weathering analogs for martian rocks and meteorites. American Mineralogist, vol. 103: pg. 502 – 516, doi: 10.2138/am-2018-6193

Aufaristama, M., Höskuldsson, A., Ulfarsson, M. O., Jónsdóttir, I., Thordarson, T., 2020. Lava flow roughness on the 2014 – 2015 lava flow-field at Holuhraun, Iceland, derived from airborne LiDAR and photogrammetry. Geosciences, vol. 10, no. 4: 125, doi: 10.3390/geosciences10040125

Cai, Y., Fa, W., 2020. Meter-scale topographic roughness of the Moon: the effect of small impact craters. Journal of Geophysical Research: Planets, 125, doi: 10.1029/2020JE006429

Campbell, B. A., Shepard, M. K., 1996. Lava flow roughness and depolarized radar scattering. Journal of Geophysical Research, vol. 101, no. E8: pg. 18,941 – 18,951.

Cao, W., Cai, Z., 2018. Improved multiscale roughness algorithm for lunar surface. IEEE Journal of Selected Topics in Applied Earth Observations and Remote Sensing, vol. 11, no. 7, pp. 2336-2345, doi: 10.1109/JSTARS.2018.2822297.

Cashman, K. V., Thornber, C., Kauahikaua, J. P., 1999. Cooling and crystallization of lava in open channels, and the transition of pāhoehoe lava to ‘a‘ā. Bulletin of Volcanology, vol 61, pg. 306 – 323.

Deliège, A., leyntssens, T., Nicolay, S., 2017. Planetary and Space Science, vol. 136, pg. 46 – 58, doi: 10.1016/j.pss.2016.12.008

Dierking, W., 1999. Quantitative roughness characterization of geological surfaces and implications for radar signature analysis. IEEE Transactions on Geoscience and Remote Sensing, vol. 37, no. 5, pg. 2397 - 2412

Duraiswami, R. A., Dole, G., Bondre, N., 2003. Slabby pāhoehoe from the western Deccan Volcanic Province: evidence for incipient pāhoehoe-aa transitions. Journal of Volcanology and Geothermal Research, vol. 121, pg. 195 – 217, doi:10.1016/S0377-0273(02)00411-0

Duvall, M. S., Hench, J. L., Rosman, J. H., 2019. Collapsing complexity: quantifying multiscale properties of reef topography. Journal of Geophysical Research: Oceans, vol 124, pg. 5021 – 5038, doi: 10.1029/2018JC014859

Fonstad, M. A., Dietrich, J. T., Courville, B. C., Jensen, J. L., Carbonneau, P. E., 2013. Topographic structure from motion: a new development in photogrammetric measurement. Earth Surface Processes and Landforms, vol. 38, pg 421 – 430, doi:10.1002/esp.3366

Garry, W. B., Hughes, S. S., Kobs Nawotniak, S. E., Wheeley, P. L., Lim, D. S. S., Heldmann, J. L., the FINESSE team, 2017. Planetary exploration of lava tubes with lidar at Craters of the Moon, Idaho. Abstract : 1207 presented at 2017 Lunar and Planetary Science Conference, Houston, TX, 20 – 24 March.

Garvin, J. B., Frawley, J. J., Abshire, J. B., 1999. Vertical roughness of Mars from the Mars Orbiter Laser Altimeter. Journal of Geophysical Research Letters, vol. 26, no. 3, pg. 381 – 384.

National Park Service (NPS) Geologic Resources Inventory (GRI) program, 2014. Unpublished Digital Geologic Map of portions of Craters of the Moon National Monument and

Preserve, Idaho (NPS, GRD, GRI, CRMO, COTM digital map) adapted from four U.S. Geological Survey Geologic Quadrangle Maps by Kuntz, Champion, and Lefebvre (1989, 1989, 1989, and 1990).

Greely, R., 1982. The Snake River Plain, Idaho: Representative of a new category of volcanism. Journal of Geophysical Research Letters, vol. 87, no. B4, pg. 2705-2712.

Greeley, R., Spudis, P. D., 1981. Volcanism on Mars. Reviews of Geophysics and Space Physics, vol. 19, no. 1, pg. 13 – 41.

Gregg, T. K. P., 2017. Patterns and processes: subaerial lava morphologies: a review. Journal of Volcanology and Geothermal Research, vol. 342, pg. 3 – 12, doi.org/10.1016/j.jvolgeores.2017.04.022

Grohmann, C. H., Smith, M. J., Riccomini, C., 2011. Multiscale Analysis of Topographic Surface Roughness in the Midland Valley, Scotland. IEEE Transactions on Geoscience and Remote Sensing, VOL. 49, NO. 4, doi: 10.1109/TGRS.2010.2053546

Guilbaud, M.-N., Self, S., Thordarson, T., Blake, S., 2005. Morphology, surface structures, and emplacement of lava produced by Laki, A. D. 1783 – 1784. Geological Society of America Special Paper 396, pg. 81 – 102, doi: 10.1130/2005.2396(07).

Guilbaud, M.-N., Blake, S., Thordarson, T., Self, S., 2007. Role of Syn-eruptive Cooling and Degassing on Textures of Lavas from the AD 1783 - 1784 Laki Eruption, South Iceland. Journal of Petrology, vol. 48, no. 7, pg. 1265 – 1294, doi:10.1093/petrology/egm017

Harris, A. J. L., Rowland, S. K., Villeneuve, N., Thordarson, T., 2017. Pāhoehoe, ʻaʻā, and block lava: an illustrated history of the nomenclature. Bulletin of Volcanology, vol. 79, no. 7, DOI 10.1007/s00445-016-1075-7

Hauber, E., Bleacher, J., Gwinner, K., Williams, D., Greeley, R., 2009. The topography and morphology of low shields and associated landforms of plains volcanism in the Tharsis region of Mars. Journal of Volcanology and Geothermal Research, vol. 185, pg. 69–95, doi:10.1016/j.jvolgeores.2009.04.015

M. R. Henriksen, Manheim, M. R., Burns, K. N., Seymour, P., Speyerer, E. J., Deran, A., Boyd, A. K., Howington-Kraus, E., Rosiek, M. R., Archinal, B. A., Robinson, M. S., 2017. Extracting accurate and precise topography from LROC narrow angle camera stereo observations. Icarus vol. 283, pg. 122 – 137, doi: 10.1016/j.icarus.2016.05.012

Hon, K., Kauahikaua, J., Denlinger, R., Mackay, K., 1994. Emplacement and inflation of pāhoehoe sheet flows: observations and measurements of active lava flows on Kilauea Volcano, Hawaii. Geological Society of America Bulletin, v. 106, p. 351-370.

Hughes, S. S., Smith, R. P., Hackett, W. R., Anderson, S. R., 1999. Mafic Volcanism and Environmental Geology of the Eastern Snake River Plain, Idaho. Mafic Volcanism and Environmental Geology of the Eastern Snake River Plain, Idaho. Guidebook to the Geology of Eastern Idaho: Idaho Museum of Natural History, p. 143-168.

Hughes, S. S., Wetmore, P. H., Casper, J. L., 2002. Evolution of Quaternary Tholeiitic Basalt Eruptive Centers on the Eastern Snake River Plain, Idaho. Tectonic and Magmatic Evolution of the Snake River Plain Volcanic Province: Idaho Geological Survey Bulletin 30.

Hughes, S. S., Haberle, C. W., Kobs Nawotniak, S. E., Sehlke, A., Brent Garry, W. B., Elphic, R. C., Payler, S. J., Stevens, A. H., Cockell, C. S., Brady, A. L., Heldmann, J. L., Lim, D. S. S., 2019. Basaltic Terrains in Idaho and Hawaiʻi as Planetary Analogs for Mars Geology and Astrobiology. Astrobiology, vol. 19, doi: 10.1089/ast.2018.1847.

Keszthelyi, L., Thordarson, T., McEwen, A., Haack, H., Guilbaud, M.-N., Self, S., Rossi, M. J., 2004. Icelandic analogs to Martian flood lavas. Geochemistry, Geophysics, Geosystems, vol. 5, doi:10.1029/2004GC000758.

Kirk, R. L., Howington-Kraus, E., Rosiek, M. R., Anderson, J. A., Archinal, B. A., Becker, K. J., Cook, D. A., Galuszka, D. M., Geissler, P. E., Hare, T. M., Holmberg, I. M., Keszthelyi, L. P., Redding, B. L., Delamere, W. A., Gallagher, D., Chapel, J. D., Eliason, E. M., King, R., McEwen, A. S., 2008. Journal of Geophysical Research, VOL. 113, doi:10.1029/2007JE003000.

Korzeniowska, K., Pfeifer, N., Landtwing, S., 2018. Mapping gullies, dunes, lava fields, and landslides via surface roughness. Geomorphology vol. 301, pg. 53 – 67.

Kreslavsky, M., Head, J. W., 2000. Kilometer-scale roughness of Mars: results from MOLA data analysis. Journal of Geophysical Research, vol. 105, no. EII, pg. 26,695 – 26,711.

Kuntz, M. A., Champion, D. E., Spiker, E. C., Lefebvre, R. H., McBroome, L. A., 1982. The Great Rift and the evolution of the Craters of the Moon lava field, Idaho. Cenozoic Geology of Idaho: Idaho Bureau of Mines and Geology Bulletin 26, pg. 423 – 437.

Kuntz, M.A., Skipp, B., Champion, D.E., Gans, P.B., Van Sistine, D.P., and Snyders, S.R., 2007. Geologic map of the Craters of the Moon 30’ x 60’ quadrangle, Idaho. U.S. Geological Survey Scientific Investigations Map 2969.

Kuntz, M. A., 1992. A model-based perspective of basaltic volcanism, eastern Snake River Plain, Idaho. Regional Geology of Eastern Idaho and Western Wyoming: Geological Society of America Memoir 179.

Lemenkova, P., 2019. K-means Clustering in R Libraries fclusterg and ffactoextrag for Grouping Oceanographic Data. International Journal of Informatics and Applied Mathematics, vol. 2, no. 1, pg. 1 – 26.

Leon, J. X., Roelfsema, C. M., Saunders, M. I., Phinn, S. R., 2015. Measuring coral reef terrain roughness using “Structure-from Motion” close-range photogrammetry. Geomorphology, vol. 242, pg. 21 – 28, doi: 10.1016/j.geomorph.2015.01.030.

Lescinsky, D. T., Skoblenick, S. V., Mansinha, L., 2007. Automated identification of lava flow structures using local Fourier spectrum of digital elevation data. Journal of Geophysical Research, vol. 112, doi:10.1029/2006JB004263.

Lipkaman, L. J., Gregg, T. K. P., 2003. A’a versus Pahoehoe on Mars, Venus, and Earth: What do Fractal Dimensions Actually Reveal? Abstract : 1389 presented at 2003 Lunar and Planetary Science Conference, Houston, TX, 17 – 21 March.

Lipman, P. W., Banks, N. G., 1987. Aa flow dynamics, Mauna Loa 1984. U.S. Geological Survey Professional Paper 1350, ch. 57.

Macdonald, G. A., 1953. Pāhoehoe, aa, and block lava. American Journal of Science, vol. 251, pg. 169 – 1919.

McCurry, M., Hayden, K. P., Morse, L. H., Mertzman, S., 2008. Genesis of post-hotspot, A-type rhyolite of the Eastern Snake River Plain volcanic field by extreme fractional crystallization of olivine tholeiite. Bulletin of Volcanology, vol. 70, pg. 361 – 383, doi: 10.1007/s00445-007-0143-4

McHenry, L. J., Richardson, C. D., Hinman, N. W., 2010. Sulfate minerals, hematite, and silica in Craters of the Moon, Idaho basaltic lava tubes: a potential analog for Mars. Abstract : 1469 presented at 2010 Lunar and Planetary Science Conference, Houston, TX, 1 - 5 March.

Morris, A. R., Anderson, F. S., Mouginis-Mark, P. J., Haldemann, A. F. C., Brooks, B. A., Foster, J.,, 2008. Roughness of Hawaiian volcanic terrains. Journal of Geophysical Research, vol. 113, doi:10.1029/2008JE003079.

Neish, C. D., Hamilton, C. W., Hughes, S. S., Kobs Nawotniak, S., Garry, W. B., Skok, J. R., Elphic, R. C., Schaefer, E., Carter, L. M., Bandfield, J. L., Osinski, G. R., Lim, D., Heldmann, J. L., 2017. Terrestrial analogues for lunar impact melt flows. Icarus, vol. 281, pg. 73 – 89, doi: 10.1016/j.icarus.2016.08.008.

Neish, C. D., 2016, personal communication.

Orosei, R., Bianchi, R., Coradini, A., Espinasse, S., Federico, C., Ferriccioni, A., Gavrishin, A. I., 2003. Self-affine behavior of Martian topography at kilometer scale from Mars Orbiter Laser Altimeter data. Journal of Geophysical Research, vol. 108, no. E4, 8023, doi:10.1029/2002JE001883.

Ozuomba, S., Enyenihi, H. J., Kalu, C., 2018. Program to determine the terrain roughness index using path profile data sampled at different moving window sizes. International Journal of Computer Applications, vol. 182, no. 34, pg. 34 – 41.

Peterson, D. W., Tilling, R. I., 1980. Transition of basaltic lava from pāhoehoe to aa, Kilauea volcano, Hawaii: field observations and key factors. Journal of Volcanology and Geothermal Research, vol. 7, pg. 271 – 293.

Pierce, K. L., Morgan, L. A., 1992. The track of the Yellowstone hot spot: volcanism, faulting, and uplift. Regional Geology of Eastern Idaho and Western Wyoming: Geological Society of America Memoir 179.

Plescia, J. B., 1993. An assessment of volatile release from recent volcanism in Elysium, Mars. Icarus, vol. 104, pg. 20 – 32.

Potter, K.E., Champion, D.E., Duncan, R.A., Shervais, J.W., 2019. Volcanic stratigraphy and age model of the Kimama deep borehole (Project Hotspot): evidence for 5.8 million years of continuous basalt volcanism, central Snake River Plain, Idaho. Geosphere, vol. 15, no. 3, pg. 736–758, doi:10.1130/GES01679.1

Richardson, C. D., Hinman, N. W., McHenry, L. J., Kotler, J. M., Knipe, D. L., Scott, J. R., 2012. Secondary sulfate mineralization and basaltic chemistry of Craters of the Moon National Monument, Idaho: potential Martian analog. Planetary and Space Science, vol. 65, pg. 93 – 103, doi: 10.1016/j.pss.2012.02.002

Rosenburg, M. A., Aharonson, O., Head, J. W., Kreslavsky, M. A., Mazarico, E., Neumann, G. A., Smith, D. E., Torrence, M. H., Zuber, M. T., 2011. Global surface slopes and roughness of the Moon from the Lunar Orbiter Laser Altimeter. Journal of Geophysical Research, vol. 116, no. E02001, doi:10.1029/2010JE003716.

Rossi, M. J., Gudmundsson, A., 1996. The morphology and formation of flow-lobe tumuli on Icelandic shield volcanoes. Journal of Volcanology and Geothermal Research, vol. 72, pg. 291 – 308.

Rousseeuw, P. J., 1987. Silhouettes: a graphical aid to the interpretation and validation of cluster analysis. Journal of Computational and Applied Mathematics, vol. 20, pg 53 – 65.

Rowland, S. K., Walker, G. P. L., 1990. Pāhoehoe and aa in Hawaii: volumetric flow rate controls the lava structure. Bulletin of Volcanology, vol. 52, pg. 615 – 628.

Rowland, S. K., Walker, G. P. L., 1987. Toothpaste lava: characteristics and origin of a lava structural type transition between pāhoehoe and aa. Bulletin of Volcanology, vol. 49, pg. 631 – 641.

Self, S., Keszthelyi, L., Thordarson, T., 1998. The Importance of pāhoehoe. Annual Review of Earth and Planetary Science, vol. 26, pg. 81 – 110.

Sehlke, A., Whittington, A., Robert, B., Harris, A., Gurioli, L., Médard, E., 2014. Pāhoehoe to `a`a transition of Hawaiian lavas: an experimental study. Bulletin of Volcanology, vol. 76, no. 876, doi: 10.1007/s00445-014-0876-9

Shepard, M. K., Campbell, B. A., Bulmer, M. H., Farr, T. G., Gaddis, L. R., Plaut, J. J., 2001. The roughness of natural terrain: a planetary and remote sensing perspective. Journal of Geophysical Research, vol. 106, no. E12, pg. 32,777 – 32,795.

Smith, M. W., Carrivick, J. K., Quincey, D. J., 2016. Structure form motion photogrammetry in physical geography. Progress in Physical Geography, vol. 40, 247 – 275.

Steinley, D., 2006. K-means clustering: a half-century synthesis. British Journal of Mathematical and Statistical Psychology, vol. 59, pg. 1 – 34.

Stout, M. Z., Nicholls, J., Kuntz, M. A., 1994. Petrological and mineralogical variations in 2500 – 2000 yr B.P. lava flows, Craters of the Moon lava field, Idaho. Journal of Petrology, vol. 35, pg. 1681 – 1715.

Tolometti, G. D., Neish, C. D., Orsinski, G. R., Hughes, S. S., Kobs Nawotniak, S. E., 2020. Interpretations of lava flow properties from radar remote sensing data. Planetary and Space Science, vol. 190, doi: 10.1016/j.pss.2020.104991.

Turcotte, D. L., 1997. Fractals and Chaos in Geology and Geophysics, Cornell University, New York, 2nd ed., doi: 10.1017/CBO9781139174695

Thompson, D. R., Abbey, W.,, Allwood, A., Bekker, D., Bornstein, B., Cabrol, N. A., Castaño, R., Chien, S. A., Doubleday, J., Estlin, T., Foil, G., Fuchs, T., Howarth, D., Ortega, K., Wagstaff, K. L., 2013. TextureCam: A Smart Camera for Microscale, Mesoscale, and Deep Space Applications. Abstract : 2209 presented at 2013 Lunar and Planetary Science Conference, Houston, TX, 18 - 22 March.

Vaucher, J., Baratoux, D., Mangold, N., Pinet, P., Kurita, K., Grégoire, M., 2009. The volcanic history of central Elysium Planitia: implications for martian magmatism. Icarus, vol. 204, pg. 418 – 442, doi: 10.1016/j.icarus.2009.06.032

Wagstaff, K. L., Thompson, D. R., Abbey, W., Allwood, A., Bekker, D. L., Cabrol, N. A., Fuchs, T., Ortega, K., 2013. Smart, texture-sensitive instrument classification for in situ rock and layer analysis. Geophysical Research Letters, vol. 40, pg. 4188–4193, doi:10.1002/grl.50817

Walker, G. P. L., 1991. Structure, and origin by injection of lava under surface crust, of tumuli, “lava rises”, “lava-rise pits”, and “lava-inflation clefts” in Hawaii. Bulletin of Volcanology, vol. 53, pg. 546 – 558, doi: 10.1007/BF00298155

Walker, G. P. L., 2009. The endogenous growth of pāhoehoe lava lobes and morphology of lava-rise edges. Special Publications of IAVCEI, Studies in volcanology: the legacy of George Walker, vol. 2, pg 17 – 32.

Westoby, M. J., Brasington, J., Glasser, N. F., Hambrey, M. J., Reynolds, J. M., 2012. ‘Structure-from-Motion’ photogrammetry: A low-cost, effective tool for geoscience applications. Geomorphology, vol. 179, pg. 300 – 314, doi: 10.1016/j.geomorph.2012.08.021

Whelley, P. L., Garry, W. B., Hamilton, C. W., Bleacher, J. E., 2017. LiDAR-derived surface roughness signatures of basaltic lava types at the Muliwai a Pele Lava Channel, Mauna Ulu, Hawai‘i. Bulletin of Volcanology, vol. 79, doi: 10.1007/s00445-017-1161-5

Wu, J., Yang, Q., Li, Y., 2018. Partitioning of Terrain Features Based on Roughness. Remote Sensing, vol 10.

APPENDIX: AREA RATIO AND RMS HEIGHT CODES

AreaRatio

```
program area_ratio


implicit none

real :: z, avg, sumIn, zone, Area, flat, pid, areaWin, area2d
real*8 :: x, y, xi, yi, ydiff, xdiff, abDist, bcDist, caDist, s, localArea
real*8 :: adDist, cdDist, acDist
real*8 :: sumTest
real :: win_width
real*8, allocatable, dimension (:,:,:) :: input !note: input values are (x, y, z, RMS)
. Combined input and RBS arrays to save on repetetive memory use
real*8, dimension(3) :: a, b, c, d
integer :: i, j, m, n, num, x_count, y_count, linecount, y_winsteps, x_winsteps, p, l,
 k
integer, dimension(9) :: orientI, orientJ
character(30):: junk
real*8 :: avg_ydiff, avg_xdiff, wind_width
integer :: wind_cells_y, wind_cells_x, halfWind
integer :: ymax, ymin, xmax, xmin

open(unit=20, file="smooth.txt", status="old")
open(unit=22, file="smooth_ar_3m_1.csv", status="new")

wind_width = 3.

num=0
x_count=0
y_count=0
xi=0.
yi=0.
ydiff = 0.
xdiff = 0.

read(20,*) junk

do
    read(20,*,END=35) zone, pid, z, x, y
    num = num+1
    if (y .ne. yi) then
        y_count = y_count+1
        if (y_count.ne.1)then
            ydiff = ydiff + abs(yi-y)
        endif
        yi=y
    endif
    if (x .gt. xi) then
        x_count = x_count+1
        if (x_count.ne.1)then
            xdiff = xdiff + abs(xi-x)
        endif
        xi=x
    endif
enddo
35 continue

print*, "total dataset size (x,y):", xdiff, ydiff, "total number of cells (x,y):", x_c
ount, y_count

avg_ydiff = ydiff/y_count
avg_xdiff = xdiff/x_count
print*, "average cell size (x,y):", avg_xdiff, avg_ydiff

if ((avg_xdiff.le.avg_ydiff).and.(wind_width.lt.(3*avg_ydiff))) then
```

AreaRatio

```
        print*, "Error: minimum window size must be greater than:", (3*avg_ydiff), "me
ters"
        goto 36
elseif ((avg_xdiff.gt.avg_ydiff).and.(wind_width.lt.(3*avg_xdiff))) then
        print*, "Error: minimum window size must be greater than:", (3*avg_xdiff), "me
ters"
        goto 36
elseif ((wind_width.gt.(ydiff-(avg_ydiff*2))).and.(ydiff.ge.xdiff)) then
        print*, "Error: minimum window size must be greater than:", (ydiff-(avg_ydiff*
2)), "meters"
        goto 36
elseif ((wind_width.gt.(xdiff-(avg_xdiff*2))).and.(xdiff.gt.ydiff)) then
        print*, "Error: minimum windows size must be greater than:", (xdiff-(avg_xdiff
*2)), "meters"
        goto 36
endif

wind_cells_y = wind_width/avg_ydiff
wind_cells_x = wind_width/avg_xdiff
print*, "cells per window (x,y):", wind_cells_x, wind_cells_y


allocate(input(y_count, x_count, 4))

rewind(20)
read(20,*) junk

input = 0.
do i=1,y_count
    do j=1,x_count
        read(20,*) zone, pid, input(i,j,3), input(i,j,1), input(i,j,2)
    enddo
enddo

if (mod(wind_cells_y,2).ne.1) wind_cells_y = wind_cells_y + 1
if (mod(wind_cells_x,2).ne.1) wind_cells_x = wind_cells_x +1

xmax = x_count - (wind_cells_x/2)
xmin = (wind_cells_x/2 + 1)
ymax = y_count - (wind_cells_y/2)
ymin = (wind_cells_y/2 + 1)
!print*, "edges (x,y):", xmin, ymin, xmax, ymax


!l = 0
!k = 0
halfWind = (wind_cells_x-1)/2
!print*, "halfwind = ", halfWind

!move center of window
do l = xmin, xmax
        do k = ymin, ymax
                areaWin = 0.

!                print*, "halfWind+1, wind_cells_x - halfWind = ", halfWind+1, wind_ce
lls_x - halfWind

                !skip holes
!                if (input(l,k,3).eq.-99999) then
!                        input(l,k,4) = -99999
 !                       GOTO 87

!                else
                        !find the planar area
                        area2d = abs(input(l-halfWind,k,2) - input(l+halfWind,k,2))
```

AreaRatio

```
                        area2d = area2d * abs(input(l,k-halfWind,1) - input(l,k+halfWin
d,1))

                       ! areaWin = 0.
                         !look across window
                         do m = l - halfWind, l + (halfWind - 1)
                                 do n = k - halfWind, k + (halfWind - 1)

                                         !establish each vertex
                                         a = [input(m,n,1), input(m,n,2), input(m,n,3)]
                                         b = [input(m,n+1,1), input(m,n+1,2), input(m,n
+1,3)]
                                         c = [input(m+1,n+1,1), input(m+1,n+1,2), input
(m+1,n+1,3)]
                                         d = [input(m+1,n,1), input(m+1,n,2), input(m+1
,n,3)]


                                         !print*, "a = ", a
                                         !print*, "b = ", b
                                         !print*, "c = ", c
                                         !print*, "d = ", d
                                         !skip this moving window if any vertex
                                         !is a hole
                                         if (a(3).le.0 .or. b(3).le.0 .or. c(3).le.0 .o
r. d(3).le.0) then
!
                                                 avg = (a(3) + b(3) + c(3) + d(3)
                                                areaWin = -99999
                                                GOTO 87
                                         else


                                                !find distance between each vertex

                                                abDist = (abs(a(1)-b(1))**2 + abs(a(2)
-b(2))**2 + abs(a(3)-b(3))**2)**0.5
                                                bcDist = (abs(b(1)-c(1))**2 + abs(b(2)
-c(2))**2 + abs(b(3)-c(3))**2)**0.5
                                                caDist = (abs(a(1)-c(1))**2 + abs(a(2)
-c(2))**2 + abs(a(3)-c(3))**2)**0.5
                                                adDist = (abs(a(1)-d(1))**2 + abs(a(2)
-d(2))**2 + abs(a(3)-d(3))**2)**0.5
                                                cdDist = (abs(c(1)-d(1))**2 + abs(c(2)
-d(2))**2 + abs(c(3)-d(3))**2)**0.5


                                                !print*, "abDist = ", abDist
                                                !print*, "bcDist = ", bcDist
                                                !print*, "caDist = ", caDist
                                                !print*, "adDist = ", adDist
                                                !print*, "cdDist = ", cdDist

                                                !calculate area of upper triangle
                                                s = (abDist + bcDist + caDist)/2
                                                !print*, "s - ", s

                                                localArea = (s* ((s-abDist) * (s-bcDis
t) * (s-caDist)))**0.5

                                                !print*, "loc area1= ", localarea

                                                areaWin = areaWin + localArea
                                                !print*, "area win = ", areaWin

                                                !calculate area of lower triangle
                                                s = (caDist + adDist + cdDist)/2
                                                !print*, "s = ", s
```

AreaRatio

```
                                                localArea = (s*((s-caDist) * (s-adDist
) * (s-cdDist)))**0.5
                                                !print*, "loc area2= ", localArea

                                                areaWin = areaWin + localArea
                                                !print*, "areaWin = ", areawin

                                        endif


                                enddo
!                                87 continue
                        enddo
!                 endif
                        87 continue
                        !find the area ratio
                        if (areaWin.le.0) then
                                input(l,k,4) = -99999
                        else
!                                input(l,k,4) = areaWin / area2d
                                input(l,k,4) = area2d / areaWin
                                !print*, "areaWin = ", areaWin
                                !print*, "area2d = ", area2d
                                !print*, "area ratio=", input(l,k,4)
                        endif


!                 endif

                 enddo
enddo


write(22,*) "X", ",", "Y", ",", "Z", ",","AreaRatio"

linecount = 0
do i=1,y_count
    do j=1,x_count
        write(22,*) input(i,j,1), ",", input(i,j,2), ",", input(i,j,3), ",", input(i,j
,4)
        linecount = linecount+1
    enddo
enddo

36 continue

close(20)
close(22)

end program area_ratio
```

RMS

```
program rms_SKN
!Code for calculating RMS values based on a 3x3 cell window
implicit none


!Variables for reading input files
real :: zone
real*8 :: x, y, z
integer :: pid
character(30) :: read_input
!variables for identifying input file dimensions
integer :: num, y_count, x_count
real*8 :: xi, yi
!Variables for RMS Calculation Loops
real*8, allocatable, dimension (:,:,:) :: input
integer :: i, j
!Variables for RMS Calculation
real*8 :: sumIn, rms, z_avg
real :: hole, z_count
integer :: tot
!Variables for adaptable window size loops
real*8 :: ydiff, xdiff, wind_width, avg_xdiff, avg_ydiff
integer :: wind_cells_x, wind_cells_y, cellsx, cellsy
integer :: ymax, ymin, xmax, xmin, k, l, cellstartx, cellstarty, cellendx, cellendy


!-----------------------------------------------
!Establish the file names/types that will be input and output
!-----------------------------------------------
open(unit=20, file="hwys2_2m.txt", status="old")!Data file being input
open(unit=22, file="hwys2_2m_20220224.csv", status="new")

!-----------------------------------------------
!Set initial variable values
!-----------------------------------------------

wind_width = 7.      !width in meters for moving window


num=0 !Variable for which line in the input datafile that the loop is on
x_count=0 !Variable for identifying  the number of cells in the y-dimension
y_count=0 !Variable for identifying  the number of cells in the x-dimension
xi=0. !Variable to make sure values aren't repeated
yi=0. !Variable to make sure values aren't repeated
xdiff = 0. !variable for establishing the size of the dataset in the x direction, in m
eters
ydiff = 0. !variable for establishing the size of the dataset in the y direction, in m
eters
hole = -99999.!data to input for holes in dataset


!-----------------------------------------------
!Read file and identify/allocate cell dimensions
!-----------------------------------------------
read(20,*) read_input
do
    read(20,*,END=35) zone, pid, z, x, y !Header Names
    num = num+1
    if (y .ne. yi) then  !identify the number of cells in the y-dimension
        y_count = y_count+1
                if (y_count.ne.1) then !eliminate first value, so that initial UTM val
ue is not added
                        ydiff = ydiff + abs(yi-y)
                endif
        yi=y
```

RMS

```
    endif
    if (x .gt. xi) then  !identify the number of cells in the x-dimension
        x_count = x_count+1
                if (x_count.ne.1) then !eliminate first value, so that initial UTM val
ue is not added
                xdiff = xdiff + abs(xi-x)
                endif
        xi=x
    endif
enddo



35 continue
print*, "total dataset size (x,y):", xdiff, ydiff, "total number of cells (x,y):", x_c
ount, y_count
!Calculate moving window logistics
avg_ydiff = ydiff/y_count !average difference between y values
avg_xdiff = xdiff/x_count !average difference between x values
print*, "average cell size (x,y):", avg_xdiff, avg_ydiff


!-----------------------------------------------
!End code if the window size is too small or too big for the dataset
!-----------------------------------------------
if ((avg_xdiff.le.avg_ydiff).and.(wind_width.lt.(3*avg_ydiff))) then
        print*, "Error: Minnimum window size must be greater than:", (3*avg_ydiff), "m
eters"
        goto 36
elseif ((avg_xdiff.gt.avg_ydiff).and.(wind_width.lt.(3*avg_xdiff))) then
        print*, "Error: Minnimum window size must be greater than:", (3*avg_xdiff), "m
eters"
        goto 36
elseif ((wind_width.gt.(ydiff-(avg_ydiff*2))).and.(ydiff.ge.xdiff)) then
        print*,"Error: Minnimum window size must be greater than:", (ydiff-(avg_ydiff*
2)), "meters"
        goto 36
elseif ((wind_width.gt.(xdiff-(avg_xdiff*2))).and.(xdiff.gt.ydiff)) then
        print*,"Error: Minnimum window size must be greater than:", (xdiff-(avg_xdiff*
2)), "meters"
        goto 36
endif

!-----------------------------------------------
!Calculates how many cells are in the moving window
!-----------------------------------------------
wind_cells_y = wind_width/avg_ydiff !Set as integer value to use in loop, and so resul
ts will be approximate
wind_cells_x = wind_width/avg_xdiff !Set as integer value to use in loop, and so resul
ts will be approximate
print*, "cells per window (x,y):", wind_cells_x, wind_cells_y

!Establish dimension sizes for array
allocate(input(y_count, x_count, 4))!allocate array size

rewind(20)
read(20,*) read_input

!-----------------------------------------------
!Transfer input data values to array
!-----------------------------------------------
input = 0. !Initially populate values with zero
do i=1,y_count !Read input file and populate array
    do j=1,x_count
        read(20,*) zone, pid, input(i,j,3), input(i,j,1), input(i,j,2)
```

RMS

```
    enddo
enddo !here

!-----------------------------------------------
!Make sure moving window has an odd set of cell dimensions (needs a center cell)
!-----------------------------------------------
if (mod(wind_cells_y,2).ne.1) wind_cells_y = wind_cells_y + 1
if (mod(wind_cells_x,2).ne.1) wind_cells_x = wind_cells_x + 1

!-----------------------------------------------
!Set edges for the calculations
!-----------------------------------------------
xmax = x_count - (wind_cells_x/2)
xmin = (wind_cells_x/2 + 1)
ymax = y_count - (wind_cells_y/2)
ymin = (wind_cells_y/2 + 1)
print*, "edges (x,y):", xmin, ymin, xmax, ymax

!-----------------------------------------------
!Complete RMS calculations for each cell, except skip those with hole(-99999) values
!input(:,:,1)= x, input(:,:,2)=y, input(:,:,3)=elevation input(:,:,4) = RMS
!-----------------------------------------------
do i = ymin,ymax !Start loop 1/2 moving window + 1 offset from edges
        do j = xmin,xmax !Start loop 1/2 moving window + 1 offset from edges
                sumIn = 0. !sum of squared cell values
                tot = 0 !total number of values
                z_avg = 0 !the average of the Z values within the window
                z_count = 0 !the number of Z values within the window

                if (input(i,j,3).eq.hole) then !do not do calculation for holes in dat
a set
                        input(i,j,4) = hole

                else !Calculate the RMS value for each cell (holes are skipped)
                        cellstarty = i - (wind_cells_y/2) !Top of window
                        cellstartx = j - (wind_cells_x/2) !Left of window
                        cellendy =  i + (wind_cells_y/2) !Bottom of window
                        cellendx = j + (wind_cells_y/2) !Right of window

                        do k = cellstarty, cellendy !Start on top of window
                                do l = cellstartx, cellendx !Start on left
                                        if ((input(k,l,3)).ne.hole) then
                                                z_avg = z_avg + input(k,l,3)
                                                z_count = z_count + 1
                                        endif
                                enddo
                        enddo

                        z_avg = z_avg / z_count


                        do k = cellstarty, cellendy !Start on top of window and work d
own
                                do l = cellstartx, cellendx !Start on left of window a
nd work right
                                        if ((input(k,l,3)).ne.hole) then
                                                sumIn = sumIn + ((input(k,l,3) - z_avg
) **2)
                                                tot = tot + 1
                                        endif
                                enddo
                        enddo
                        rms = sqrt(sumIn/(tot-1)) !Sum of squared values divided by nu
mber of values
                        input(i,j,4) = rms
```

RMS

```
                    endif
            enddo
enddo
!-----------------------------------------------------
!Write the final calculations into a .csv file
!-----------------------------------------------------
write(22,*) "X", ",", "Y", ",", "Z", ",","RMS"
do i=1,y_count
            do j=1,x_count
                    if(input(i,j,4).gt.0)then !Write values that have RMS calculations
                                write(22,*) input(i,j,1), ",", input(i,j,2), ",", input(i,j,3)
, ",", input(i,j,4)
                    endif
            enddo
enddo


36 continue

close(20)
close(22)

end program RMS_SKN
```